NASA Technical Memorandum 81896

NASA-TM-81896 19810008107

LABORATORY MEASUREMENTS OF SELECTED OPTICAL, PHYSICAL, CHEMICAL, AND REMOTE-SENSING PROPERTIES OF FIVE WATER MIXTURES CONTAINING CALVERT CLAY AND A NONFLUORESCING DYE

J.W. USRY, C.H. WHITLOCK, L.R. POOLE, AND W.G. WITTE, JR.

JANUARY 1981

NASA
National Aeronautics and Space Administration

Langley Research Center
Hampton, Virginia 23665

SUMMARY

Remotely sensed spectral reflectance, optical properties, and limited chemical and physical properties were measured in the laboratory for three mixtures containing filtered, deionized water and Calvert clay and two mixtures containing filtered, deionized water, Calvert clay, and a nonfluorescing dye. These data were measured and are being presented for possible use as inputs to analytical models to predict upwelled reflectance values.

Optical parameters include color, spectral variations of beam attenuation coefficient, absorption coefficient, scattering coefficient, single-scattering albedo, volume-scattering function, backscattering coefficient, and diffuse-attenuation coefficient. Parameters obtained by remote sensing include apparent upwelled radiance and reflectance at wavelengths between 400 nm and 800 nm. Physical and chemical properties of the mixtures include total suspended solids, nonfluorescing dye concentration, iron concentration, and particle size distribution.

Total suspended solids concentrations ranged from 6.1 ppm to 24.3 ppm and sizes ranged between 1.5 μm and 10 μm with the most frequently occurring size less than 2 μm. Iron concentration was less than 1 percent of the total suspended solids. Nonfluorescing dye concentrations of the mixtures were 20 ppm and 40 ppm. Attenuation coefficients for the five mixtures ranged from 4.8 m^{-1} to 21.3 m^{-1}.

Variations in volume scattering function with phase angle were typical. Variations in attenuation and absorption coefficient with wavelength were similar for the mixtures without the dye. Attenuation coefficients of the mixtures with the dye increased for wavelengths less than 600 nm due to the strong absorption peak near 500 nm. Reflectance increased as the concentration of Calvert clay increased and peaked near 600 nm. The nonfluorescent dye decreased the magnitude of the peak, but had practically no effect on the variation of reflectance for wavelengths greater than 640 nm. The spectral variations of the mixtures with the dye were significantly different from those mixtures without the dye for wavelengths less than 600 nm.

INTRODUCTION

Aircraft and satellite data have shown that remote-sensing techniques can be used to detect differences in water properties. Various types of particulates and dissolved compounds give rise to changes in water color and near infrared upwelled radiation characteristics. The optical mechanisms for these changes are not well understood and remain a critical limiting factor in the reliable interpretation of remote-sensing data. A number of optical physics models have been developed for relatively clear ocean waters (see references 1-5). These models may quantitatively explain the optical mechanisms which cause the remote-sensing signal, but they have not been tested in highly turbid waters because of the lack of experimental data.

To advance the state of remote-sensing technology, the Langley Research Center has initiated a laboratory and field experiments program for the measurement of turbid water parameters including in situ optical, chemical, and physical properties and remotely sensed spectral radiance and reflectance. It is

expected that data from these experiments may aid in the testing and verification of various optical models which calculate upwelled reflectance with given values for various underwater optical parameters. Results of a field experiment to measure some of these parameters were reported in reference 6.

The purpose of this paper is to present results of a laboratory experiment in which Calvert clay was mixed with a nonfluorescing dye in a large water tank. These data were measured specifically for use as inputs to analytical models to predict upwelled radiance values. Preliminary models were developed by the Mitre Corporation. A description of the modeling approach and results of a sensitivity study concerning the design of the experimental facility were reported in references 7 and 8. Another study dealing with variations in the characteristics of the backscattered radiance as a result of changes in the scattering function has been reported in reference 9.

Optical parameters presented in this paper consist of water color and spectral variations (between 450 nm and 800 nm) of beam attenuation coefficient (α), absorption coefficient (a), scattering coefficient (s), single scattering albedo ($\tilde{\omega}_0$), volume-scattering function ($\beta(\theta)$), backscattering coefficients ((b*), (b*/a), (b*/s)), and diffuse attenuation coeffieient (k). Remotely sensed parameters to be shown consist of apparent upwelled radiance, L_z, and reflectance, ρ_z, at wavelengths, λ, between 400 nm and 800 nm. Measured properties of the water samples consisted of total suspended solids, nonfluorescing dye concentration, iron concentration, and particle size distribution.

SYMBOLS

a	absorption coefficient, m^{-1}
B	fraction of s scattered in back hemisphere from $\pi/2$ to π, = b*/s
b*	backscattering coefficient, m^{-1}
F	function of s scattered in forward hemisphere from 0 to $\pi/2$, = 1 - B
K	diffuse attenuation coefficient, m^{-1}
L_{so}	upwelled spectral radiance above water surface from 100 percent diffuse reflector, mW/cm^2 - sr - nm
L_z	apparent upwelled spectral radiance above water surface, mW/cm^2 - sr - nm
s	scattering coefficient, m^{-1}
α	beam attenuation coefficient, m^{-1}
$\beta(\theta)$	volume scattering function, m^{-1} sr^{-1}

λ	wavelength, nm
ρ_z	apparent upwelled spectral reflectance above water surfaces, percent of input (relative to a 100 percent diffuse reflector)
θ	scattering or phase angle, deg
θ_o	solar zenith angle, deg
σ	standard deviation of measurement error
$\tilde{\omega}_o$	single scattering albedo, = s/α

LABORATORY AND EQUIPMENT

Figure 1 is a sketch of the laboratory arrangement. The water tank volume is approximately 14.7 m^3. Generally, for convenience, 11,600 liters of water are used in the tank for an experiment. The inside walls of the tank are painted black to minimize reflections. In previous experiments, several types of base water have been used in the tank including water pumped from the Back River (ref. 10), artificial seawater (ref. 11), and filtered and deionized water (ref. 12). During an experiment, the circulation system keeps the water in motion so that particles up to 100 μm (specific gravity less than 2.6) are kept in suspension (ref. 12).

The solar simulator spectral input to the water surface is similar to the air-mass-zero Sun (ref. 13). Test data supplied by the manufacturer of the simulator show the energy distribution between 400 nm and 800 nm to be within ±10 percent of the air-mass-zero Sun and total intensity within ±1.4 percent for all wavelengths. The rapid-scanning spectrometer views the illuminated surface through a telephoto lens so that less than 3 percent of the surface area illuminated by the solar simulator beam is in the field of view of the spectrometer. Results of a study reported in references 7 and 8 showed that this characteristic adequately simulates actual field conditions.

A number of instruments were utilized for the optical measurements in this study. A summary of the different instruments and their performance capabilities is given in table 1.

Optical measurements of α and $\beta(\theta)$ at small angles ($\theta = 0.37^o$, 0.75^o, and 1.5^o) were made every 50 nm for 450 nm $\leq\lambda\leq$ 800 nm with a spectral resolution of 10 nm. The Langley-developed Small Angle Scattering Meter (SASM) was used for these α and $\beta(\theta)$ measurements. The SASM operates on the same optical principle as the Scripps Institute of Oceanography ALSCAT instrument (see ref. 14). To achieve high-turbidity capability, SASM measurements are made using various lengths of sample laboratory cells rather than in situ as ALSCAT. Repetitive measurements indicate that the standard deviation (σ) of the SASM measurements was better than ±5 percent for α and ±12 percent for $\beta(\theta)$.

Measurements of a at wavelengths and spectral resolution identical to those of SASM were made with the Langley SPectral Absorption Coefficient Instrument (SPACI). This instrument used the measurement approach of reference 15,

and is described in more detail by Cherdak and Friedman (ref. 15). A series of unpublished laboratory experiments conducted with SPACI and SASM indicate that SPACI may be used to measure spectral variation of the absorption coefficient for turbid waters having $0.1\ m^{-1} \leq a \leq 15\ m^{-1}$. Repetitive tests and analyses indicate a standard deviation of $\pm 0.1\ m^{-1}$ for $0.1\ m^{-1} \leq a \leq 1\ m^{-1}$ and ± 10 percent for $1\ m^{-1} \leq a \leq 15\ m^{-1}$ in the SPACI measurements.

Large-angle measurements of $(\beta(\theta))$ were made with a Brice-Phoenix (BP) light scattering photometer which had been modified to give spectral data. A tungsten lamp replaced the original light source and a filter wheel system was added so that measurements could be made every 50 nm from 450 nm to 800 nm. Modifications were made to increase detector sensitivity and the range of measurement angles.

EXPERIMENTAL METHODS

Experimental procedures used were similar to procedures used in other experiments in this laboratory (refs. 10, 11, 12) and for that reason only a brief description will be given in this paper.

The water tank was filled with 11,600 liters of filtered and deionized water and the solar simulator light beam was projected into the tank as illustrated in figure 1. One hundred (100) grams of Calvert clay were added to the tank to form mixture MI-07 (see table II). This mixture was allowed to circulate for approximately 20 minutes to achieve a uniform distribution of the clay in the water column. After the clay had mixed thoroughly, the upwelled radiance was measured with the spectrometer mounted over the tank (see fig. 1). The second mixture, MI-08, was formed by adding 125 gm of Calvert clay to the first mixture, MI-07. Similar procedures were used to form the other mixtures listed in table II and to measure the upwelled radiance for each mixture. Periodically during the experiment, radiance measurements were made of the input solar spectrum using a 99 percent diffuse reflector. These measurements were used in the calculation of reflectance for each mixture.

A sample of each mixture was analyzed for selected physical and chemical properties and the results are presented in table II. Mixtures MI-10 and MI-11 were formed by adding the nonfluorescing dye without adding additional Calvert clay. Particle size ranges were obtained from Coulter analysis. Actual size distributions are shown in figure 2. Reference 17 shows results of a previous study of particle size distribution and clay mineral content of Calvert clay using pipette analysis and x-ray diffraction techniques. Reference 12 presents results of a previous experiment in this laboratory to measure radiance and reflectance spectra of Calvert clay mixed with filtered and deionized water.

Chromaticity characteristics are shown in figure 3. These were calculated from reflectance spectra and Internationale de l'Eclairage (CIE) standard functions (see ref. 18). Point S on figure 3 represents uniform spectral intensity white color.

DATA RESULTS

Spectral characteristics of beam attenuation, absorption, and scattering coefficients, α, a, and s are shown in figure 4 for all the mixtures. Volume-scattering function, $\beta(\theta)$, as a function of phase angle, θ, for wavelengths, λ, of 450, 550, 650, and 750 nm for all of the mixtures are shown in figure 5. Curves of $\beta(\theta)$ for other λ are similar and are not shown for brevity. Beam attenuation, a, and $\beta(\theta)$ were measured in increments of 50 nm between 450 and 800 nm, and values of $\beta(\theta)$ were corrected for effects of absorption along the sample path length discussed in reference 19. Spectral resolution and inaccuracies of these measurements are specified in table I and values are listed in table III.

Scattering coefficients were calculated quasi-independently by integrating values of $\beta(\theta)$ and by subtracting the absorption coefficient from the beam attenuation coefficient, i.e.,

$$s = 2\pi \int_0^{\pi} \beta(\theta) \sin \theta \, d\theta \tag{1}$$

and

$$s = \alpha - a \tag{2}$$

To perform the integration in equation (1), smooth functions of $\beta(\theta)$ as a function of phase angle, θ, for each λ were generated by computer in log space using cubic spline curve fits of the measured values of $\beta(\theta)$. Gaps in the measured values of $\beta(\theta)$ were then filled by these computed points to assist in the generation of smooth functions of $\beta(\theta) \sin \theta$ in linear space for phase angles between 0° to 180°.

For convenience, a scattering probability function, i.e.,

$$P(\theta) = \frac{2\pi}{s} \int_0^{\theta} \beta(\theta) \sin \theta \, d\theta \tag{3}$$

was defined in terms of s from equation (1). This function and the measured α were used in an analytical model of the absorption meter employing Monte Carlo simulation methods to quantify the true value of the absorption coefficient, a (see ref. 20). The measured values of a, as derived from the basic instrument equation (see ref. 20), have a systematic error which was corrected by an iterative process to yield the true value of a (see ref. 19). This was done by initializing the simulation using measured values of α and a and corrected values of $\beta(\theta)$ to compute s and $P(\theta)$ using equations (1) and (3). Using values of a from the initial computation, new values of $\beta(\theta)$, s, and $P(\theta)$ were generated. The iteration converges when changes in $P(\theta)$ are small for all angular intervals in equation (3). The resulting true values of a are then used to compute s from equation (2). Values of s computed from equations (1), s (int), and (2), s (meas), are listed in table III.

Backscatter coefficients, b^*, were computed by

$$b^* = 2\pi \int_{\pi/2}^{\pi} \beta(\theta) \sin \theta \, d\theta \qquad (4)$$

and are listed in table III and plotted in figure 6 as a function of wavelength. The uncertainty in b^* is difficult to establish since $\beta(\theta) \sin \theta$ in equation (4) is actually a function fitted to discrete measurements of $\beta(\theta)$ and θ.

Single-scattering albedo, $\tilde{\omega}_o$, characteristics were calculated from s and α. Figure 7 shows these values as a function of wavelength. All of the mixtures had a predominance of scattering at all wavelengths. Single-scattering albedo was practically constant for MI-07, MI-08, and MI-09 for all wavelengths below 700 nm. The absorption properties of water would account for the decrease in $\tilde{\omega}_o$ above 700 nm. The nonfluorescing dye absorption peak near 500 nm is apparent for MI-10 and MI-11, although scattering actually increased at all wavelengths when the dye was added to MI-09 (see fig. 4(c) also).

Variations of the ratios of backscattering coefficient to scattering coefficient and absorption coefficient with wavelength are shown in figure 8. These parameters are of interest to oceanographers as inputs to optical models. The ratios b^*/a and b^*/s are required inputs for models discussed in references 2 and 3, for example, where $b^*/s = B$ is the fraction of light scattered in the backward hemisphere.

Another parameter of interest is the diffuse attenuation coefficient K shown in figure 9. This parameter was estimated for a solar zenith angle of 15^o (incidence of solar beam to normal to water surface) using

$$K = \frac{a + b^*}{\cos \theta_o} = \frac{\alpha(1 - \tilde{\omega}_o F)}{\cos \theta_o} \qquad (5)$$

where $F = 1 - B$ and θ_o = solar zenith angle. According to reference 2, equation (5) is valid for $\tilde{\omega}_o \geq 0.6$ and should be applicable for these tests.

Radiance data were obtained from measurements made with the rapid-scanning spectrometer (see table 1). Upwelled radiance distributions with wavelength for the 99 percent diffuse reflector (white card) and for the five water mixtures are shown in figures 10 and 11. Reflectance measurements as a function of wavelength, derived by normalizing the data in figure 11 to the white card measurements of figure 10, are shown in figure 12. Spectral resolution was 6 nm for the white card measurements and 16 nm for the mixtures.

Calvert clay is red due to the iron content and this property is indicated by the trends shown in figure 12 for mixtures MI-07, MI-08, and MI-09. Also, data reported in reference 12 showed similar trends of spectral reflectance with wavelength for mixture concentrations between 4 ppm and 173 ppm and spectral resolution of 32 nm. In figure 12, the reflectance increased only slightly with λ for the mixture with the lowest concentration of clay (6.1 ppm) MI-07 for wavelengths below 600 nm. As the concentration of clay increases, the change in ρ_z with λ increases and peaks at 600 nm. Addition of the nonfluorescing dye to MI-09 did not change the reflectance significantly above λ = 600 nm but below λ = 600 nm, the shape of the curve was determined by the absorptance peak of the dye near 500 nm.

CONCLUDING REMARKS

Remotely sensed spectral reflectance, optical properties, and limited chemical and physical properties have been measured for three mixtures containing filtered, deionized water and Calvert clay and two mixtures containing filtered, deionized water, Calvert clay, and a nonfluorescing dye. Total suspended solids range from 6.1 ppm for MI-07 to 24.3 ppm for MI-11. Attenuation coefficient, α , at 550 nm increased from 4.8 m^{-1} for MI-07 to 21.3 m^{-1} for MI-11. Particle sizes for all samples were between 1.5 μm and 10 μm with the most frequently occurring size less than 2 μm.

Trends in the volume-scattering function $\beta(\theta)$, with phase angle, θ, were typical. Generally, for a specific mixture $\beta(\theta)$ decreased at the higher wavelengths but increased at all phase angles as particle count increased. Variations in α and a with wavelengths above 600 nm were similar for all five mixtures while MI-07, MI-08, and MI-09 were similar at all wavelenghts. In mixtures MI-10 and MI-11, α increased below 600 nm due to the strong absorption characteristics of the nonfluorescing dye. Variations in s with λ were similar for all mixtures. Backscattering coefficient spectra were practically invariant with λ below 700 nm and decreased slightly for $\lambda > 700$ nm. Similar trends were observed for $\tilde{\omega}_o$ and K spectra, especially for mixtures without the dye (MI-07, MI-08, and MI-09) and for b*/s spectra. However, significant spectral variations were observed in the b*/a spectra for all mixtures. Reflectance increased at all wavelengths as the concentration of Calvert clay increased. The reflectance spectra peaked near λ = 600 nm for all mixtures. The nonfluorescing dye decreased the reflectance peak value but had practically no effect for $\lambda >$ 600 nm. Below λ = 600 nm, the spectral variation of the mixture containing the nonfluorescing dye was significantly different from the other mixtures.

References

1. Gordon, H. R.: Simple Calculation of the Diffuse Reflectance of the Ocean. Applied Optics, vol. 12, no. 12, December 1973, pp. 2803-2804.

2. Gordon, H. R.; Brown, O. B.; and Jacobs, M. M.: Computed Relationships Between the Inherent and Apparent Optical Properties of a Flat Homogeneous Ocean. Applied Optics, vol. 14, no. 2, February 1975, pp. 417-427.

3. Jain, S. C.; and Miller, J. R.: Subsurface Water Parameters: Optimization Approach to Their Determination for Remotely Sensed Water Color Data. Applied Optics, vol. 15, no. 4, April 1976, pp. 886-890.

4. Morel, A.; and Prieur, L.: Analysis of Variations in Water Color. Limnology and Oceanography, vol. 22, no. 4, July 1977, pp. 709-722.

5. Plass, G. N.; Humphreys, T. J.; and Kattawar, G. W.: Color of the Ocean. Applied Optics, vol. 17, no. 9, May 1978, pp. 1432-1446.

6. Whitlock, Charles H.; et al.: Spectral Scattering Properties of Turbid Waters. Geophysical Research Letters, vol. 7, no. 1, January 1980, pp. 81-84.

7. Ghovanlou, A. H.: Analytical Model for Remote Sensing of Water Turbidity. NASA CR-145050, Sept. 1976.

8. Ghovanlou, A. H.: Radiative Transfer Model for Remote Sensing of Suspended Sediments in Water. NASA CR-145145, 1977.

9. Ghovanlou, Ali H.; Gupta, Jai N.; and Henderson, Robert G.: Determination of Scattering Functions and Their Effects on Remote Sensing of Turbidity in Natural Waters. NASA CR-145239, July 1977.

10. Usry, J. W.; Witte, William G.; Whitlock, Charles H.; and Gurganus, E. A.: Laboratory Measurements of Radiance and Reflectance Spectra of a Dilute Biosolid Waste Product. NASA TP-1401, Feb. 1979.

11. Whitlock, Charles H.; Usry, J. W.; Witte, William G.; Farmer, Franklin H.; and Gurganus, E. A.: Investigation of Effects of Background Water on Upwelled Reflectance Spectra and Techniques for Analysis of Dilute Primary-Treated Sewage Sludge. NASA TP-1446, August 1979.

12. Whitlock, Charles H.; Usry, J. W.; Witte, William G.; and Gurganus, E. A.: Laboratory Measurements of Upwelled Radiance and Reflectance Spectra of Calvert, Ball, Jordan, and Feldspar Soil Sediments. NASA TP-1039, 1977.

13. Moon, Parry: Proposed Standard Solar-Radiation Curves for Engineering Use. J. Franklin Inst., vol. 230, no. 5, Nov. 1940, pp. 583-617.

14. Austin, R. W.; and Petzold, T. J.: An Instrument for the Measurement of Spectral Attenuation Coefficient and Narrow Angle Volume-Scattering Function of Ocean Waters. Ocean Optics, vol. 64, 1975, pp. 50-61.

15. Gilbert, G. D.; Honey, R. C.; Myers, R. E.; and Sorenson, G. P.: Optical Absorption Meter. Final Report for Stanford Research Institute Project 7440, 1969.

16. Cherdak, A.; and Friedman, E.: An Absorption Coefficient Instrument for Water: Concept, Fabrication, Calibration. NASA CR-158955, 1978.

17. Chapman, Raymond S.: Particle Size and X-Ray Analysis of Feldspar, Calvert, Ball, and Jordan Soils. NASA TM X-73941, 1977.

18. Jerlov, N. G.: Optical Oceanography. Elsevier Publishing Co., (New York), 1968.

19. Petzold, T. J.: Volume Scattering Functions for Selected Waters. SIO Ref. 72-78, Visibility Lab., San Diego, CA 92151, Oct. 1972.

20. Friedman, E.; Poole, L.; Cherdak, A.; Houghton, W.: Absorption Coefficient Instrument for Turbid Natural Waters. Appl. Opt. (1980).

TABLE I.- CAPABILITIES OF OPTICAL INSTRUMENTS

INSTRUMENT	MEASURED PARAMETER	RANGE OF MEASUREMENT	INACCURACY (σ)	WAVELENGTH OF MEASUREMENT	SPECTRAL RESOLUTION
SASM[1]	α	$0.08\ m^{-1} \leq \alpha \leq 325\ m^{-1}$	<5%	400 nm to 800 nm in 50 nm increments	10 nm
SPACI[2]	a	$0.1\ m^{-1} \leq a \leq 15\ m^{-1}$	<10%a		10 nm
SASM[1]	$\beta(\theta)$	$0.375° \leq \theta \leq 1.5°$	<12%$\beta(\theta)$		10 nm
MODIFIED BP[3]	$\beta(\theta)$	$20° \leq \theta \leq 160°$	<20%$\beta(\theta)$		10 nm
RSS[4]	L_z	VARIABLE[5]	<5%L	400 nm to 800 nm in 4 nm increments	6 nm[5]

NOTES:

[1]Small Angle Scattering Meter

[2]SPectral Absorption Coefficient Instrument

[3]Brice-Phoenix Light Scattering Photometer

[4]Rapid-Scan Spectrometer

[5]Depends on instrument settings

TABLE II.- TEST-WATER CONDITIONS

MIXTURE	1	MI-07	MI-08	MI-09	MI-10	MI-11
DESCRIPTION	FILTERED DEIONIZED WATER	MIXTURE 1 PLUS 100 GM CALVERT CLAY	MIXTURE MI-07 PLUS 125 GM CALVERT CLAY	MIXTURE MI-08 PLUS 125 GM CALVERT CLAY	MIXTURE MI-09 PLUS 225 Mℓ NONFLUORESCING DYE*	MIXTURE MI-10 PLUS 225 Mℓ NONFLUORESCING DYE
Total suspended solids, ppm	0	6.1	13.1	22.2	24.2	24.3
Nonfluorescing dye concentration, ppm	0	0	0	0	20	40
Iron, mg/ℓ	-	0.07	0.12	0.19	0.18	0.24
Particle size range, μ	-	1.5 - 10	1.5 - 10	1.5 - 10	1.5 - 10	1.5 - 10
Most frequent particle size, μ	-	<2	<2	<2	<2	<2
Attenuation coefficient at 550 nm	-	4.81	9.82	14.66	18.28	21.34
Secchi disk depth, m	-	1.27	0.69	0.53	0.38	0.13
Inherent C.I.E. chromaticity (a) color (b) purity	- -	595 9	582 20	583 25	611 33	630 34

* Sauer's red color, strawberry shade. Contains: water, propylene, glycol, U.S. certified F.D.&C. red #40 and blue #1. 2.5% pure dye.

TABLE III.- OPTICAL PROPERTIES

(a) MI-07

Volume Scattering Function

SCATTERING ANGLE, DEG	Wavelength, nm 450	500	550	600	650	700	750	800
0.374	.34718E+03	.26380E+03	.20845E+03	.17024E+03	.14019E+03	.13427E+03	.11369E+03	.10277E+03
0.751	.31551E+03	.25416E+03	.20827E+03	.17943E+03	.14019E+03	.14304E+03	.11369E+03	.10277E+03
1.490	.18841E+03	.15056E+03	.12980E+03	.10223E+03	.99061E+02	.95663E+02	.80809E+02	.75539E+02
25.000	.10014E+01	.10442E+01	.10262E+01	.99318E+00	.98039E+00	.99830E+00	.96746E+00	.94390E+00
30.	.62779E+00	.64700E+00	.60984E+00	.61361E+00	.59277E+00	.59997E+00	.57440E+00	.57393E+00
45.	.21664E+00	.22445E+00	.21012E+00	.21044E+00	.21107E+00	.20954E+00	.19552E+00	.18448E+00
60.	.99175E-01	.99539E-01	.84537E-01	.10030E+00	.93108E-01	.89452E-01	.85400E-01	.82912E-01
75.	.54594E-01	.56503E-01	.45738E-01	.60771E-01	.50400E-01	.52386E-01	.47309E-01	.45504E-01
90.	.35818E-01	.36205E-01	.35378E-01	.42087E-01	.33239E-01	.34002E-01	.30189E-01	.28491E-01
105.	.28693E-01	.28495E-01	.27755E-01	.31566E-01	.26137E-01	.25402E-01	.23300E-01	.21727E-01
120.	.25323E-01	.25860E-01	.24921E-01	.29402E-01	.23080E-01	.23426E-01	.20362E-01	.19268E-01
135.	.26094E-01	.26544E-01	.24726E-01	.30582E-01	.23080E-01	.22734E-01	.20464E-01	.19370E-01
150.	.32160E-01	.32496E-01	.30296E-01	.30976E-01	.28406E-01	.28565E-01	.25022E-01	.24289E-01
155.	.40151E-01	.40694E-01	.34987E-01	.48578E-01	.33239E-01	.34496E-01	.29784E-01	.28081E-01
α	5.87	5.09	4.81	4.65	4.47	4.62	6.69	5.69
a	.82	.64	.48	.53	.49	.65	2.80	2.41
s (meas)	5.05	4.45	4.33	4.12	3.98	3.97	3.89	3.28
s (int)	5.66	5.35	5.25	4.51	4.69	4.65	4.28	4.02
b*	.19	.19	.18	.22	.17	.17	.15	.14

TABLE III.- CONTINUED

(b) MI-08

Volume Scattering Function

SCATTERING ANGLE, DEG	Wavelength, nm 450	500	550	600	650	700	750	800
0.374	.83885E+03	.65854E+03	.53144E+03	.44756E+03	.38682E+03	.35039E+03	.31043E+03	.29071E+03
0.751	.64320E+03	.52968E+03	.44580E+03	.39115E+03	.31785E+03	.33007E+03	.29973E+03	.27628E+03
1.490	.36551E+03	.30061E+03	.26291E+03	.21754E+03	.21049E+03	.20216E+03	.17085E+03	.16992E+03
25.	19694E+01	.20365E+01	.20051E+01	.18108E+01	.19773E+01	.20836E+01	.19621E+01	.18767E+01
30.	.12393E+01	.12393E+01	.12400E+01	.11306E+01	.12380E+01	.12788E+01	.12229E+01	.11799E+01
45.	.42188E+00	.43157E+00	.42302E+00	.43193E+00	.42574E+00	.43729E+00	.40245E+00	.39393E+00
60.	.19779E+00	.19499E+00	.19084E+00	.17931E+00	.19506E+00	.20032E+00	.18343E+00	.17467E+00
75.	.11120E+00	.11179E+00	.11257E+00	.11748E+00	.10955E+00	.11178E+00	.10038E+00	.96624E-01
90.	.74870E-01	.73055E-01	.72643E-01	.76935E-01	.72056E-01	.73330E-01	.65158E-01	.62155E-01
105.	.58656E-01	.56503E-01	.46813E-01	.59093E-01	.55044E-01	.55265E-01	.49188E-01	.48683E-01
120.	.53393E-01	.50177E-01	.50393E-01	.55118E-01	.49611E-01	.50079E-01	.43439E-01	.41715E-01
135.	.53393E-01	.59657E-01	.50393E-01	.52115E-01	.47562E-01	.48290E-01	.42161E-01	.40786E-01
150.	.61543E-01	.55983E-01	.54878E-01	.50613E-01	.52015E-01	.51241E-01	.43804E-01	.42087E-01
155.	.70116E-01	.58930E-01	.60242E-01	.55118E-01	.56023E-01	.56249E-01	.48549E-01	.46825E-01
α	11.52	10.50	9.82	9.53	9.09	9.06	10.83	9.66
a	1.35	1.20	1.12	1.04	.96	1.04	2.86	2.52
s (meas)	10.17	9.30	8.70	8.49	8.13	8.02	7.97	7.14
s (int)	11.02	10.75	9.97	8.81	9.21	9.36	8.15	7.97
b*	.38	.35	.35	.36	.34	.34	.30	.29

TABLE III.- CONTINUED

(c) MI-09

Volume Scattering Function

SCATTERING ANGLE, DEG	Wavelength, nm 450	500	550	600	650	700	750	800
0.374	.10022E+04	.78817E+03	.61434E+03	.52959E+03	.44573E+03	.41658E+03	.36740E+03	.32336E+03
0.751	.79186E+03	.65561E+03	.55621E+03	.49313E+03	.40374E+03	.42646E+03	.38448E+03	.35381E+03
1.490	.47959E+03	.31999E+03	.33996E+03	.27923E+03	.26994E+03	.25864E+03	.21568E+03	.20787E+03
25.	.30031E+01	.30354E+01	.30945E+01	.27559E+01	.30336E+01	.31175E+01	.29568E+01	.29907E+01
30.	.18492E+01	.19123E+01	.19360E+01	.17501E+01	.19634E+01	.19617E+01	.18382E+01	.18681E+01
45.	.65239E+00	.65641E+00	.66865E+00	.68976E+00	.66869E+00	.68618E+00	.60995E+00	.62126E+00
60.	.31510E+00	.31113E+00	.31022E+00	.28747E+00	.31624E+00	.31908E+00	.29996E+00	.28679E+00
75.	.16654E+00	.17681E+00	.17261E+00	.18452E+00	.17462E+00	.17582E+00	.15959E+00	.15682E+00
90.	.11687E+00	.11838E+00	.11818E+00	.12354E+00	.11748E+00	.11965E+00	.10611E+00	.10283E+00
105.	.91719E-01	.88786E-01	.93300E-01	.10057E+00	.90124E-01	.87909E-01	.80296E-01	.77039E-01
120.	.81364E-01	.81956E-01	.81638E-01	.91070E-01	.79583E-01	.80502E-01	.70436E-01	.68813E-01
135.	.82843E-01	.81956E-01	.81638E-01	.87903E-01	.74111E-01	.79606E-01	.72776E-01	.66927E-01
150.	.10207E+00	.10093E+00	.99520E-01	.91070E-01	.94952E-01	.97677E-01	.85226E-01	.83809E-01
155.	.11613E+00	.11610E+00	.11507E+00	.10849E+00	.11507E+00	.11803E+00	.10444E+00	.96835E-01
α	17.01	15.74	14.66	13.82	13.08	12.76	14.21	12.86
a	1.45	1.26	1.16	1.07	.99	1.08	2.83	2.56
s (meas)	15.56	14.48	13.50	12.75	12.09	11.68	11.38	10.30
s (int)	16.43	14.80	14.36	12.60	12.86	13.04	11.68	11.63
b*	.60	.59	.60	.63	.58	.59	.53	.50

TABLE III.- CONTINUED

(d) MI-10

Volume Scattering Function

SCATTERING ANGLE, DEG	Wavelength, nm 450	500	550	600	650	700	750	800
0.374	.13138E+04	.10097E+04	.83023E+03	.73203E+03	.63712E+03	.49038E+03	.52825E+03	.48151E+03
0.751	.92519E+03	.75660E+03	.65494E+03	.59361E+03	.59461E+03	.52678E+03	.47971E+03	.44226E+03
1.390	.52425E+03	.43370E+03	.38962E+03	.32695E+03	.31765E+03	.30763E+03	.25700E+03	.25337E+03
25.	.30198E+01	.32913E+01	.31601E+01	.28235E+01	.31349E+01	.32057E+01	.30633E+01	.30183E+01
30.	.19728E+01	.20073E+01	.19602E+01	.17988E+01	.19162E+01	.20230E+01	.19036E+01	.19633E+01
45.	.68017E+00	.32766E+00	.69090E+00	.74230E+00	.68907E+00	.69093E+00	.66465E+00	.65988E+00
60.	.31409E+00	.33061E+00	.32123E+00	.30588E+00	.32116E+00	.32835E+00	.30313E+00	.29769E+00
75.	.18375E+00	.15497E+00	.17813E+00	.19582E+00	.17629E+00	.18440E+00	.16396E+00	.16290E+00
90.	.11823E+00	.12029E+00	.11626E+00	.13358E+00	.11881E+00	.11905E+00	.10638E+00	.10502E+00
105.	.93300E-01	.94459E-01	.91673E-01	.10171E+00	.91212E-01	.91813E-01	.81581E-01	.78971E-01
120.	.86891E-01	.84866E-01	.83475E-01	.94116E-01	.82781E-01	.82476E-01	.72383E-01	.72025E-01
135.	.86178E-01	.85604E-01	.84220E-01	.94116E-01	.82014E-01	.83255E-01	.71903E-01	.73431E-01
150.	.10826E+00	.99625E-01	.10360E+00	.10474E+00	.10424E+00	.10426E+00	.90379E-01	.89308E-01
155.	.13034E+00	.11660E+00	.12074E+00	.12523E+00	.12494E+00	.12838E+00	.11037E+00	.11163E+00
α	21.41	23.46	18.28	15.91	15.21	14.87	16.17	14.49
a	3.53	5.96	2.56	1.38	1.16	1.33	3.01	2.74
s (meas)	17.88	17.50	15.72	14.53	14.05	13.54	13.16	11.75
s (int)	16.05	14.39	15.51	13.68	14.87	13.96	12.75	12.21
b*	.63	.62	.61	.67	.61	.62	.54	.54

TABLE III.- CONCLUDED

(e) MI-11

Volume Scattering Function

SCATTERING ANGLE, DEG	Wavelength, nm 450	500	550	600	650	700	750	800
0.374	.12956E+04	.10259E+04	.82738E+03	.73009E+03	.64063E+03	.59009E+03	.52746E+03	.47971E+03
0.751	.95393E+03	.79206E+03	.67476E+03	.61670E+03	.50311E+03	.52560E+03	.46909E+03	.43196E+03
1.490	.54361E+03	.44750E+03	.39886E+03	.34335E+03	.33619E+03	.32844E+03	.27923E+03	.27702E+03
25.	.32556E+01	.35029E+01	.32443E+01	.29547E+01	.33746E+01	.33281E+01	.31535E+01	.30922E+01
30.	.20023E+01	.21626E+01	.20295E+01	.18830E+01	.19735E+01	.21423E+01	.19581E+01	.19386E+01
45.	.70012E+00	.75312E+00	.69032E+00	.71895E+00	.69374E+00	.70082E+00	.65822E+00	.64327E+00
60.	.32556E+00	.35714E+00	.32152E+00	.29845E+00	.33294E+00	.32440E+00	.29647E+00	.29640E+00
75.	.17993E+00	.18580E+00	.17967E+00	.18681E+00	.17325E+00	.18209E+00	.16514E+00	.15942E+00
90.	.11832E+00	.12260E+00	.12075E+00	.12652E+00	.11901E+00	.11935E+00	.10538E+00	.10094E+00
105.	.91016E-01	.95948E-01	.93109E-01	.96753E-01	.89637E-01	.89515E-01	.79427E-01	.75142E-01
120.	.81914E-01	.86810E-01	.82198E-01	.90055E-01	.80593E-01	.81865E-01	.72034E-01	.67932E-01
135.	.83314E-01	.83764E-01	.80743E-01	.88566E-01	.79091E-01	.81865E-01	.71563E-01	.66170E-01
150.	.95916E-01	.92140E-01	.90199E-01	.87822E-01	.93403E-01	.90281E-01	.80999E-01	.77385E-01
155.	.10642E+00	.98232E-01	.10184E+00	.99730E-01	.10094E+00	.10635E+00	.93582E-01	.88921E-01
α	24.36	30.04	21.34	16.92	16.02	15.55	16.99	15.49
a	5.15	11.49	4.06	1.56	1.25	1.35	3.13	2.57
s (meas)	19.21	18.55	17.28	15.36	14.77	14.20	13.86	12.92
s (int)	17.96	17.19	15.57	13.95	16.63	14.32	13.48	13.24
b*	.59	.60	.58	.61	.57	.58	.51	.49

TABLE IV.- SINGLE SCATTERING ALBEDO, s/α

WAVELENGTH, NM	MI-07	MI-08	MI-09	MI-10	MI-11
450	0.86	0.88	0.91	0.84	0.79
500	0.87	0.89	0.92	0.75	0.62
550	0.90	0.89	0.92	0.86	0.81
600	0.89	0.89	0.92	0.91	0.91
650	0.89	0.89	0.92	0.92	0.92
700	0.86	0.89	0.92	0.91	0.91
750	0.58	0.74	0.80	0.81	0.82
800	0.58	0.74	0.80	0.81	0.83

TABLE V.- BACKSCATTER COEFFICIENT RATIOS

(a) b*/a

WAVELENGTH, NM	MI-07	MI-08	MI-09	MI-10	MI-11
450	0.232	0.281	0.414	0.178	0.115
500	0.297	0.292	0.468	0.104	0.052
550	0.375	0.313	0.517	0.238	0.143
600	0.415	0.346	0.589	0.486	0.391
650	0.347	0.354	0.586	0.526	0.456
700	0.262	0.327	0.546	0.466	0.430
750	0.054	0.105	0.187	0.179	0.163
800	0.058	0.115	0.195	0.197	0.191

(b) b*/s

WAVELENGTH, NM	MI-07	MI-08	MI-09	MI-10	MI-11
450	0.038	0.037	0.039	0.035	0.031
500	0.043	0.038	0.041	0.035	0.032
550	0.042	0.040	0.044	0.039	0.034
600	0.053	0.042	0.049	0.046	0.040
650	0.043	0.042	0.050	0.043	0.039
700	0.043	0.042	0.051	0.046	0.041
750	0.039	0.038	0.047	0.041	0.037
800	0.043	0.041	0.049	0.046	0.038

TABLE VI.- DIFFUSE ATTENUATION COEFFICIENT

WAVELENGTH, NM	MI-07	MI-08	MI-09	MI-10	MI-11
450	1.04	1.78	2.11	4.29	5.92
500	0.86	1.60	1.91	6.78	12.46
550	0.68	1.52	1.81	3.27	4.78
600	0.77	1.44	1.75	2.11	2.24
650	0.68	1.34	1.62	1.82	1.88
700	0.85	1.42	1.72	2.01	1.99
750	3.04	3.26	3.46	3.67	3.75
800	2.63	2.90	3.15	3.38	3.15

TABLE VII.- RADIANCE VERSUS WAVELENGTH FOR THE WHITE CARD AND EACH MIXTURE

	$L_u(\lambda)$, $\frac{mW/nm}{cm^2-sr}$					
λ, nm	WHITE CARD	MI-07	MI-08	MI-09	MI-10	MI-11
400	6.17×10^{-3}	0.073×10^{-3}	0.080×10^{-3}	0.080×10^{-3}	0.061×10^{-3}	0.066×10^{-3}
420	10.47	0.143	0.164	0.183	0.117	0.113
440	12.11	0.162	0.211	0.240	0.155	0.122
460	13.05	0.193	0.235	0.286	0.160	0.122
480	14.82	0.205	0.263	0.315	0.127	0.103
500	12.29	0.175	0.249	0.296	0.085	0.061
520	11.58	0.167	0.230	0.282	0.070	0.047
540	11.93	0.171	0.244	0.310	0.089	0.052
560	12.23	0.188	0.277	0.348	0.183	0.117
580	12.46	0.195	0.319	0.394	0.296	0.205
600	12.41	0.214	0.338	0.446	0.390	0.352
620	12.82	0.190	0.315	0.423	0.394	0.385
640	13.23	0.168	0.301	0.413	0.387	0.392
660	12.29	0.149	0.270	0.362	0.371	0.369
680	11.99	0.136	0.251	0.343	0.329	0.336
700	12.93	0.122	0.242	0.319	0.324	0.338
720	10.52	0.093	0.195	0.249	0.272	0.275
740	10.76	0.052	0.108	0.178	0.178	0.193
760	11.29	0.038	0.089	0.141	0.113	0.136
780	14.11	0.054	0.136	0.160	0.136	0.141
800	10.76	0.059	0.117	0.146	0.113	0.117

TABLE VIII.- REFLECTANCE VERSUS WAVELENGTH FOR EACH MIXTURE

λ, nm	$P_u(\lambda)$, percent				
	MI-07	MI-08	MI-09	MI-10	MI-11
400	1.13	1.30	1.30	0.97	1.13
420	1.34	1.53	1.72	1.15	1.05
440	1.32	1.73	1.98	1.24	0.99
460	1.46	1.76	2.22	1.23	0.92
480	1.42	1.74	2.09	0.88	0.67
500	1.46	2.03	2.44	0.65	0.49
520	1.47	1.99	2.42	0.60	0.43
540	1.42	2.01	2.60	0.75	0.42
560	1.55	2.29	2.86	1.47	0.98
580	1.52	2.57	3.13	2.41	1.85
600	1.69	2.74	3.63	3.14	2.82
620	1.48	2.42	3.28	3.04	3.04
640	1.29	2.27	3.10	2.95	2.95
660	1.22	2.20	2.93	3.01	3.01
680	1.17	2.09	2.84	2.75	2.84
700	0.93	1.86	2.47	2.47	2.63
720	0.86	1.81	2.38	2.57	2.57
740	0.46	1.02	1.67	1.67	1.77
760	0.35	0.80	1.24	0.97	1.24
780	0.35	0.99	1.13	0.99	0.99
800	0.56	1.12	1.39	1.02	1.12

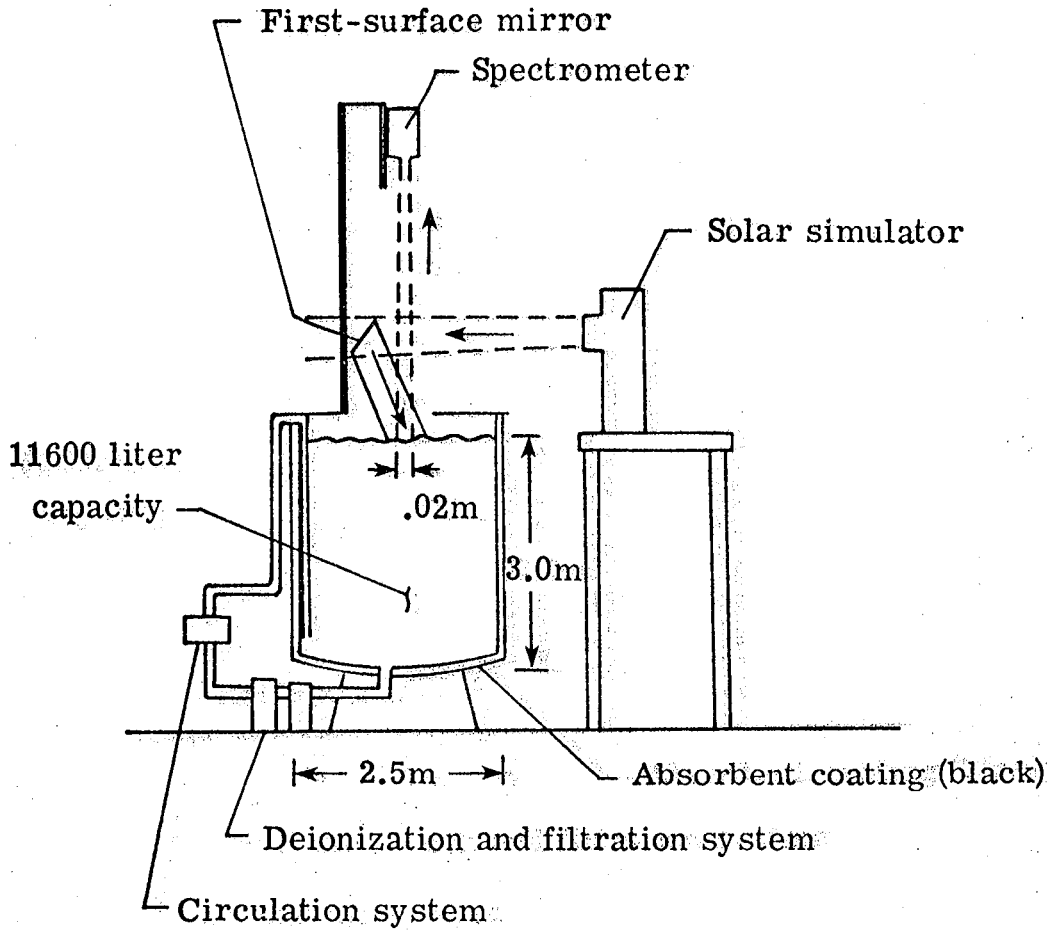

Figure 1.- Sketch of laboratory setup.

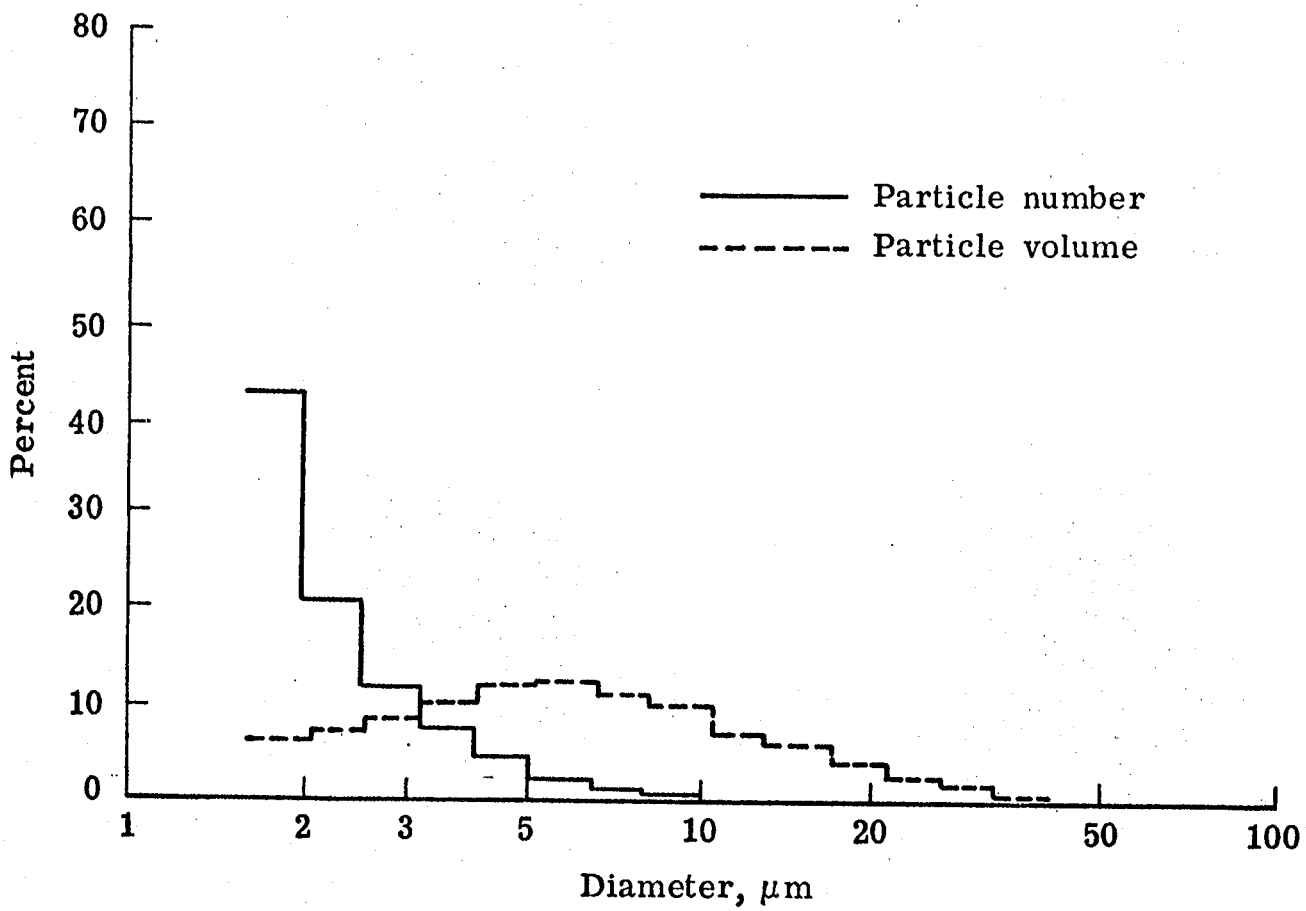

Figure 2.- Particle size distribution.

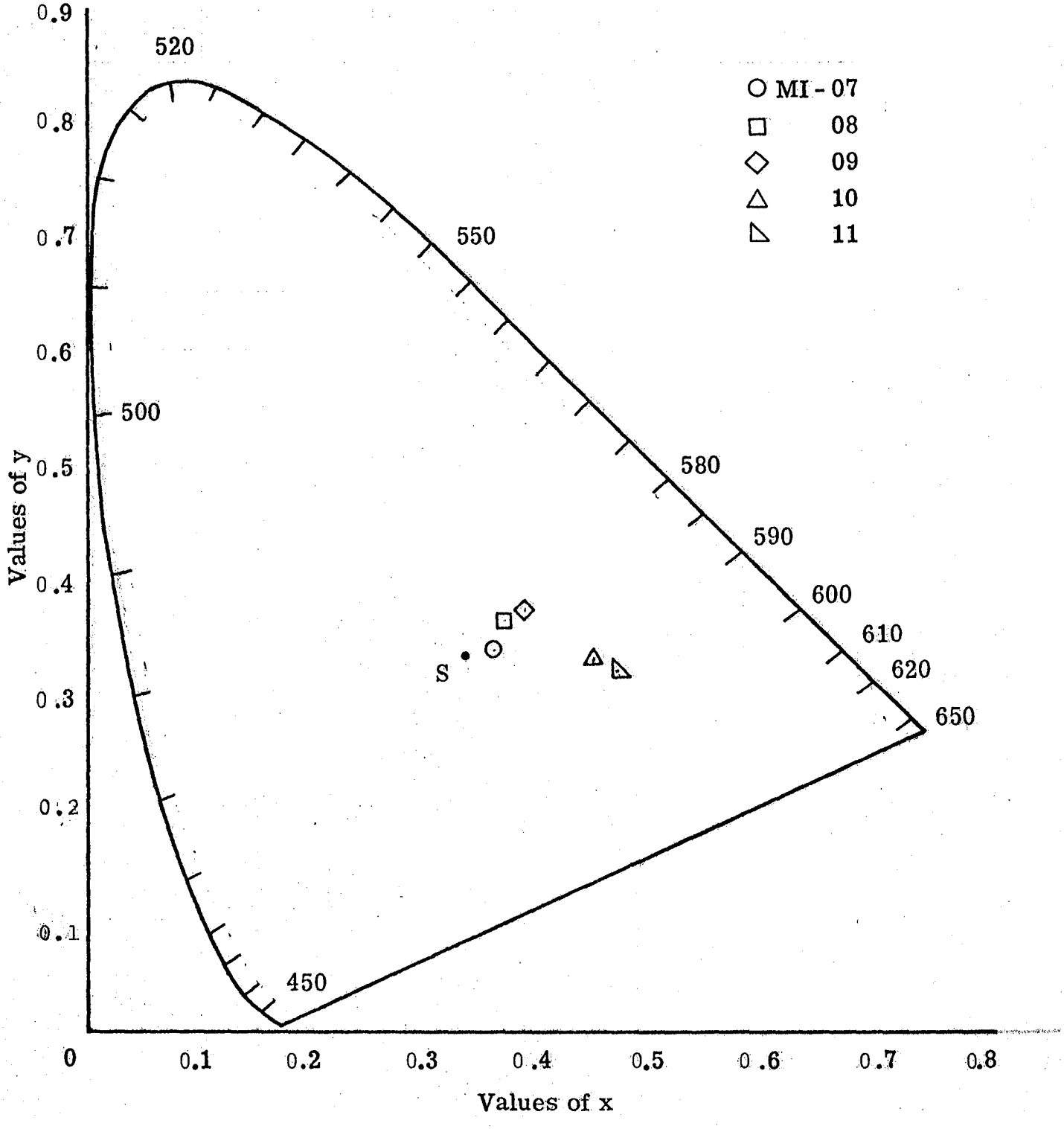

Figure 3.- C.I.E. chromaticity.

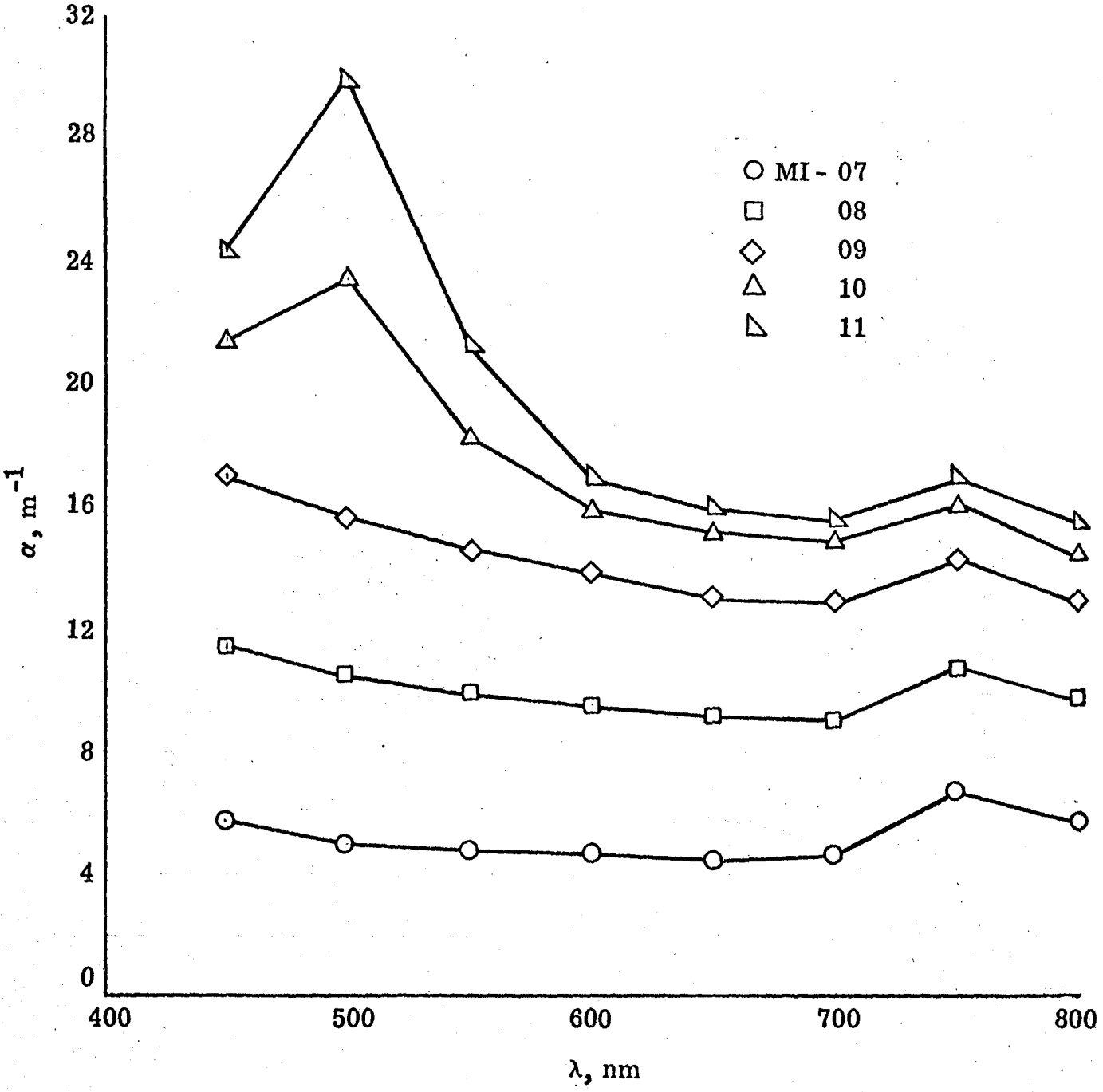

a) Attenuation coefficient

Figure 4.- Attenuation, absorption, and scattering coefficient.

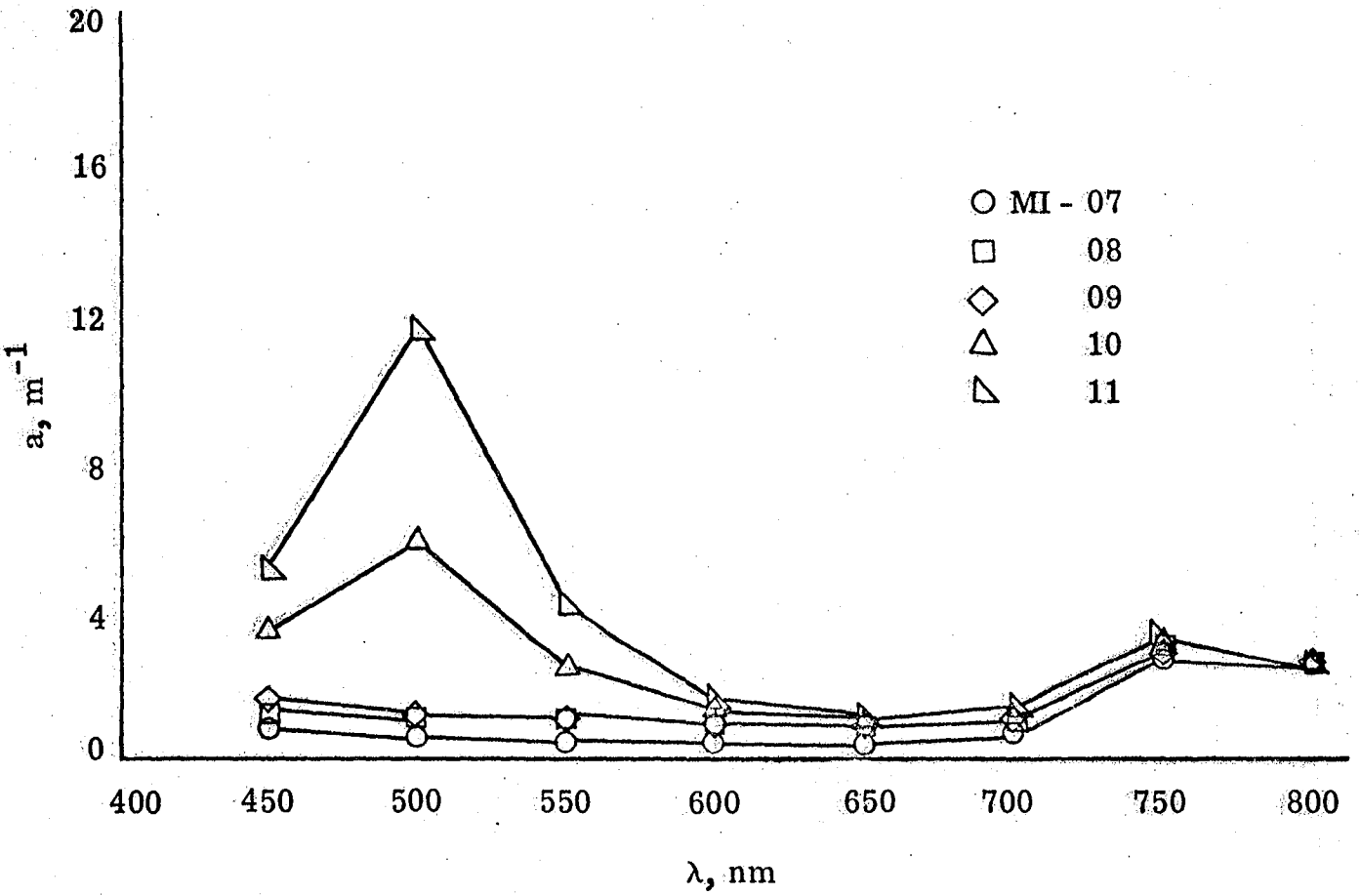

b) Absorption coefficient

Figure 4.- Continued.

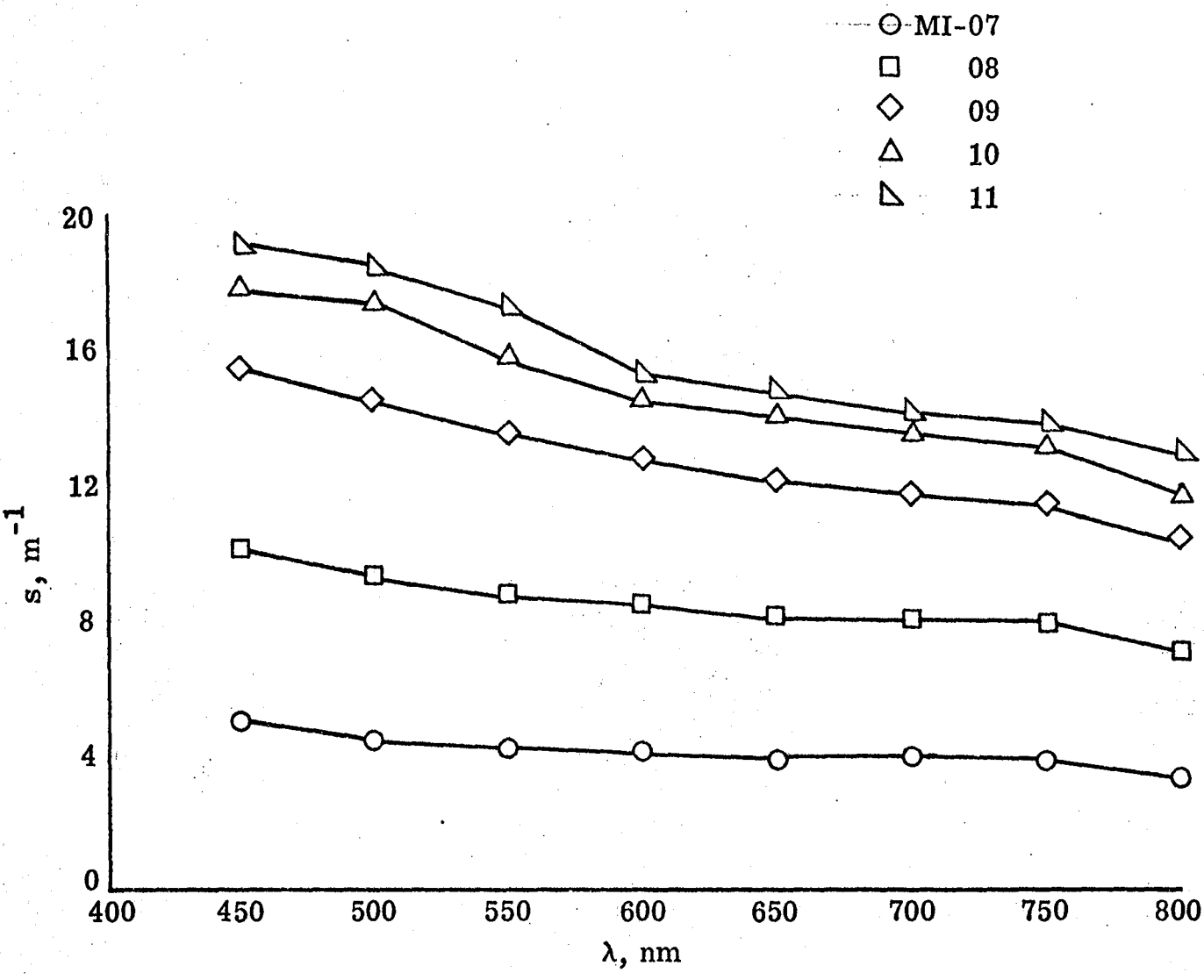

(c) Scattering coefficient

Figure 4.- Concluded.

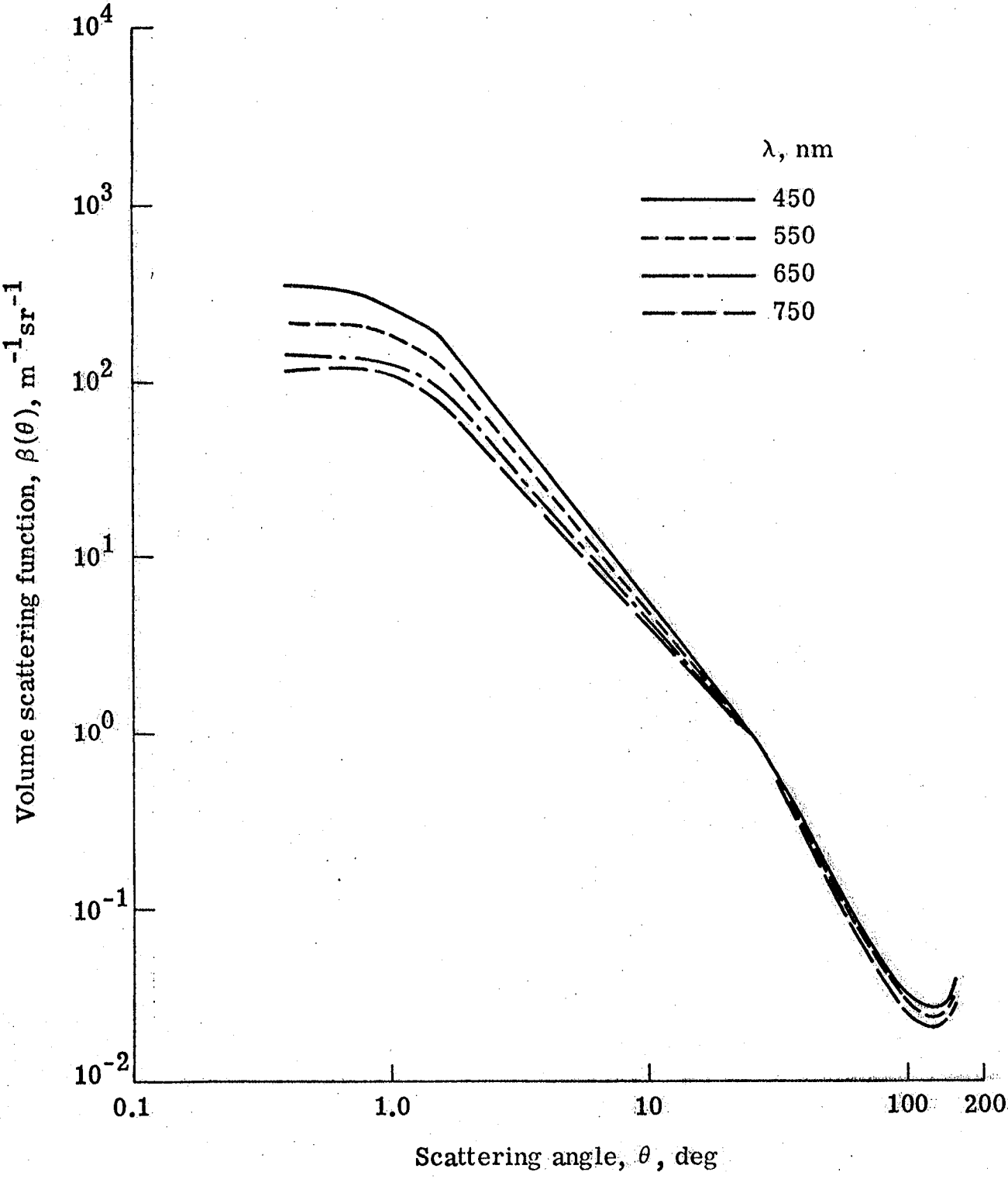

(a) Mixture MI-07

Figure 5.- Volume scattering function versus scattering angle.

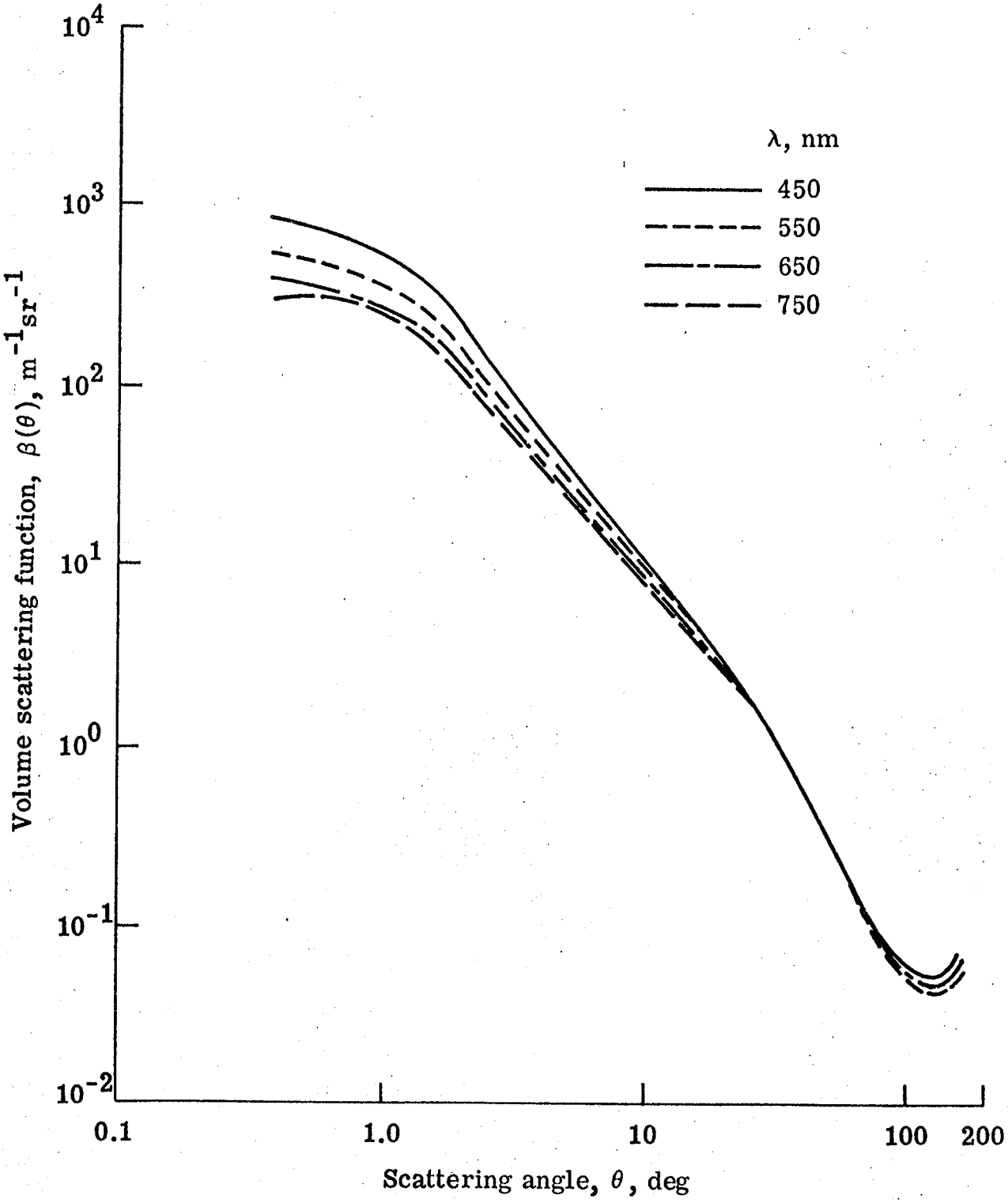

(b) Mixture MI-08

Figure 5.- continued.

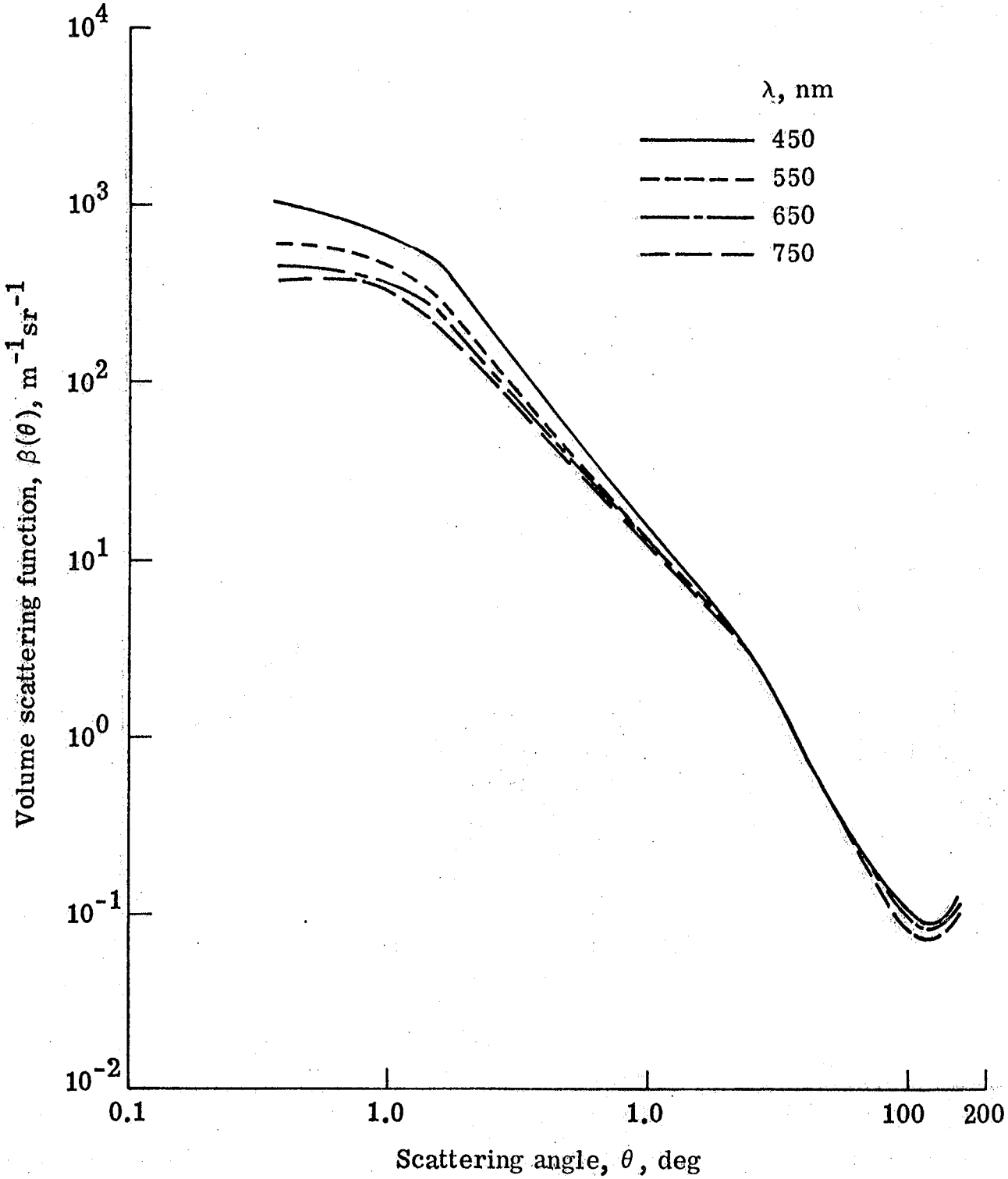

(c) Mixture MI-09

Figure 5.- continued.

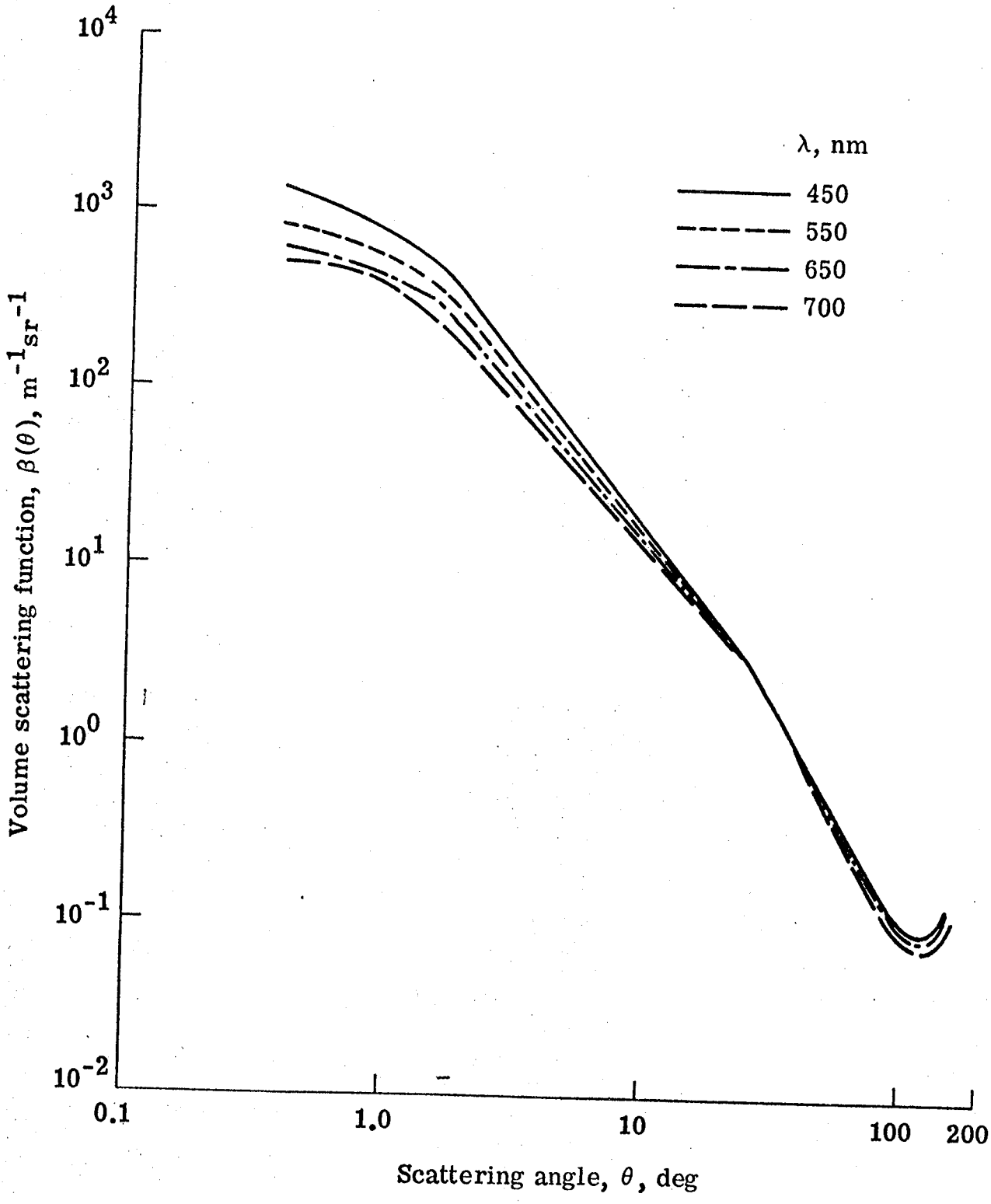

(d) Mixture MI-10

Figure 5.- Continued.

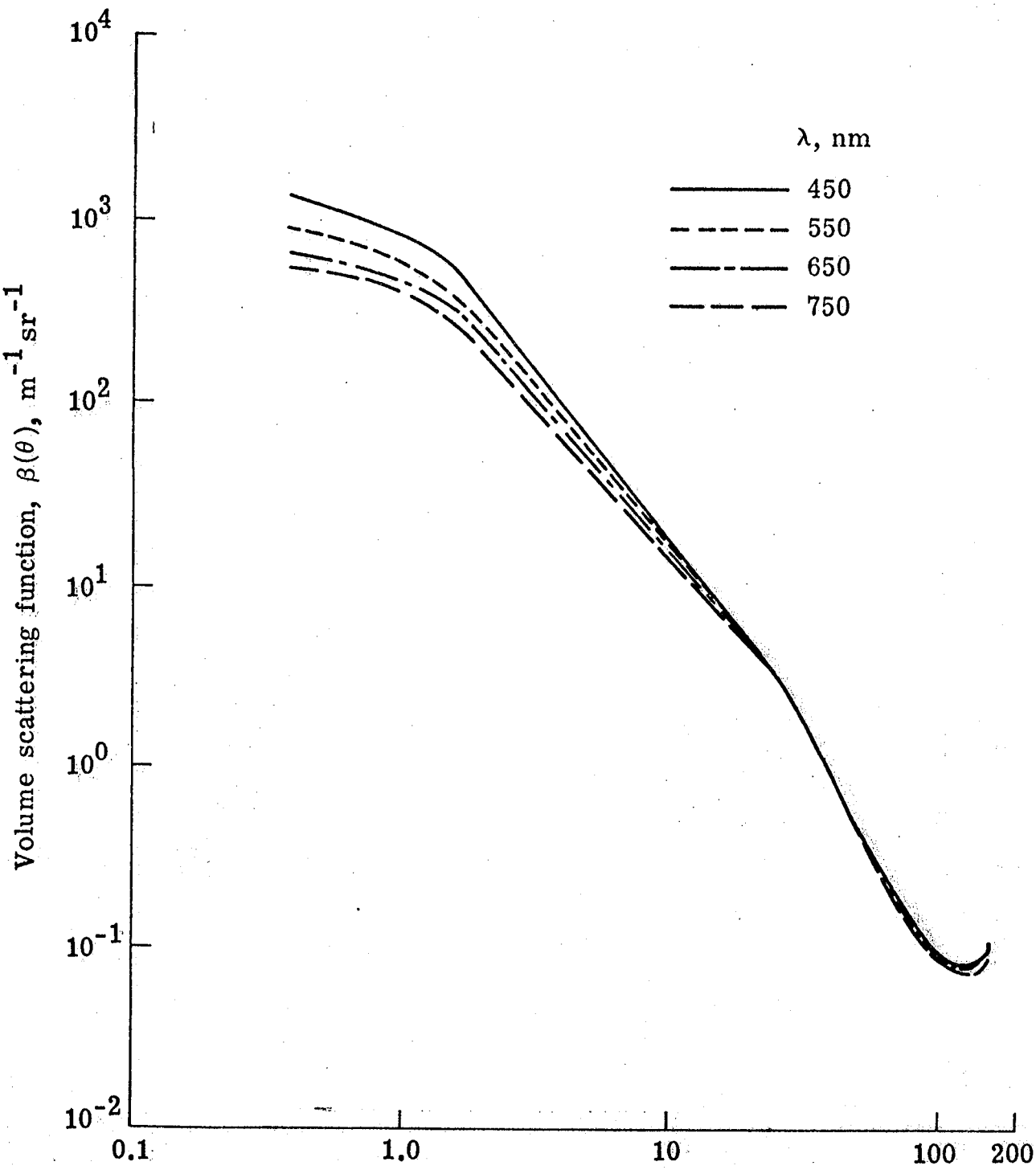

(e) Mixture MI-11

Figure 5.- continued.

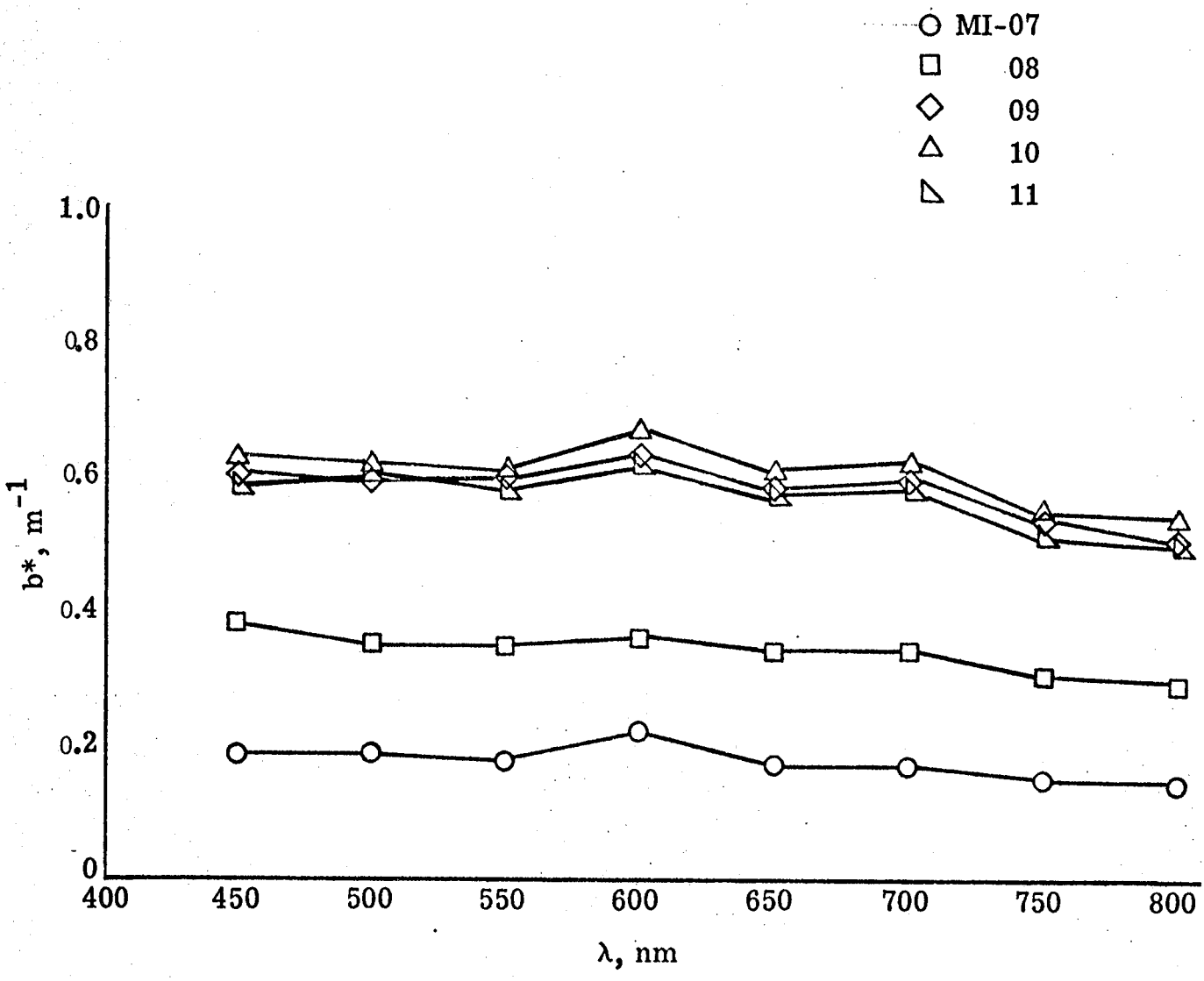

Figure 6.- Backscattering coefficient spectra.

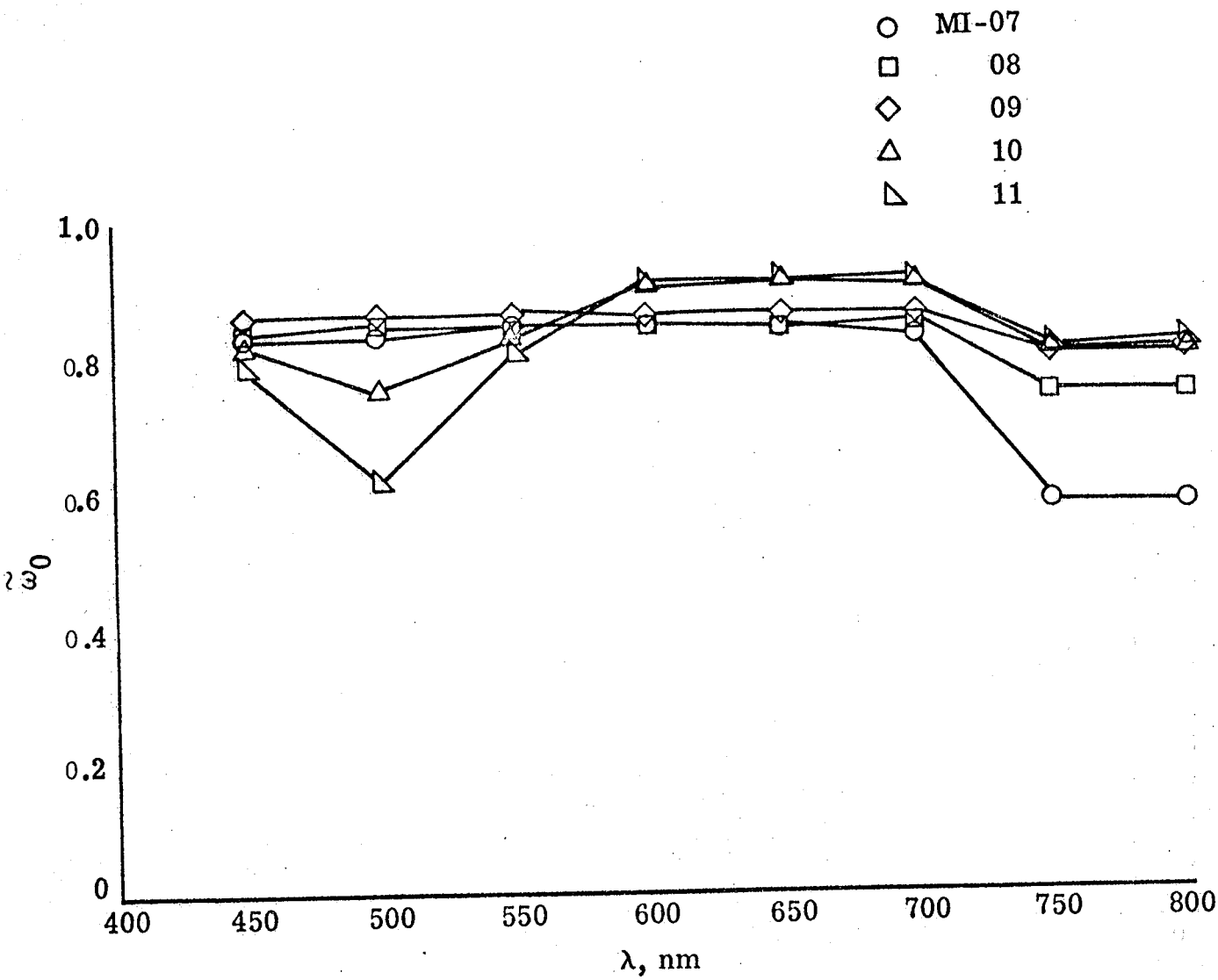

Figure 7.- Single scattering albedo spectra.

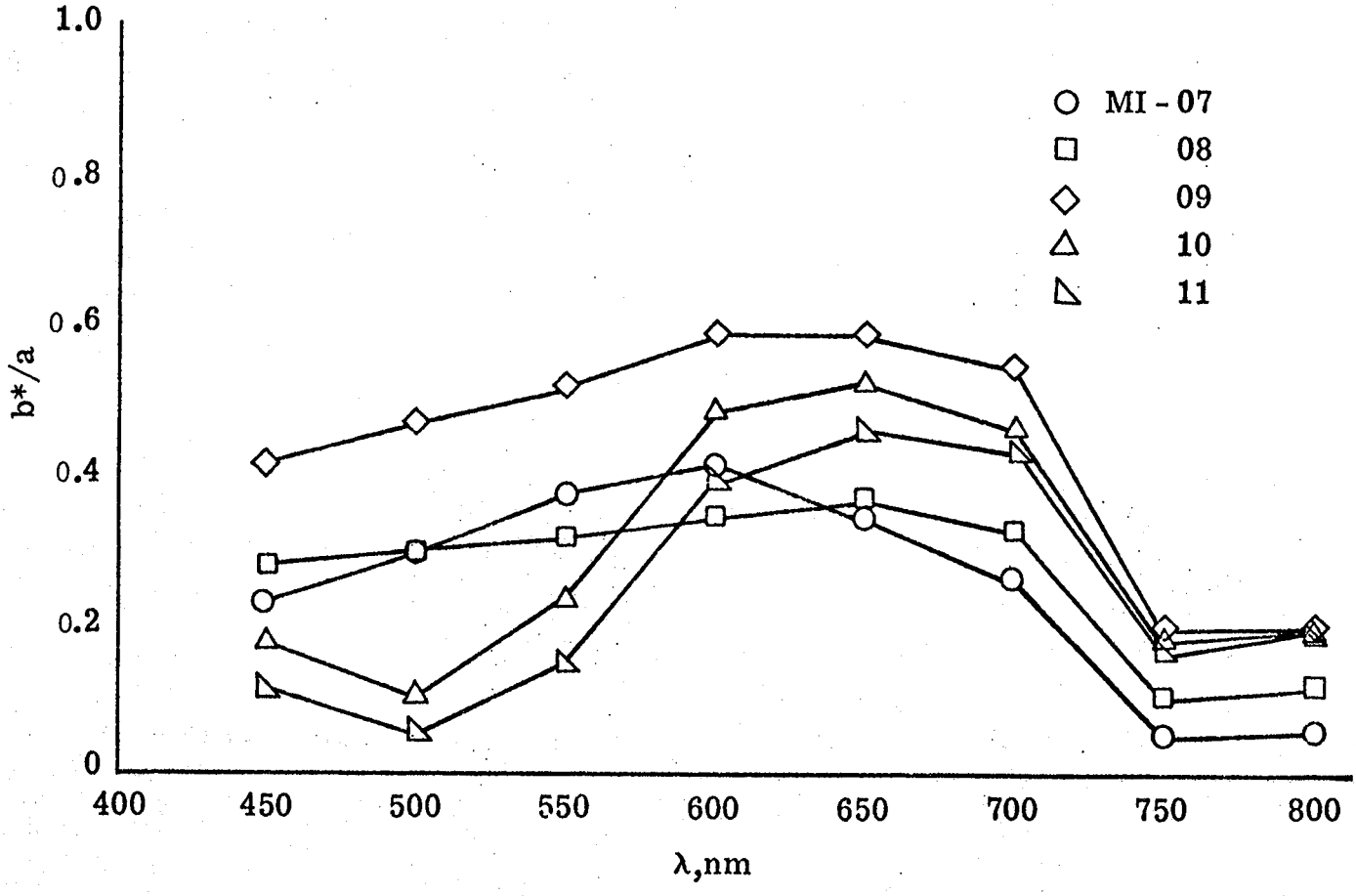

(a) b*/a

Figure 8.- Ratio of backscattering coefficient to absorption and scattering coefficient.

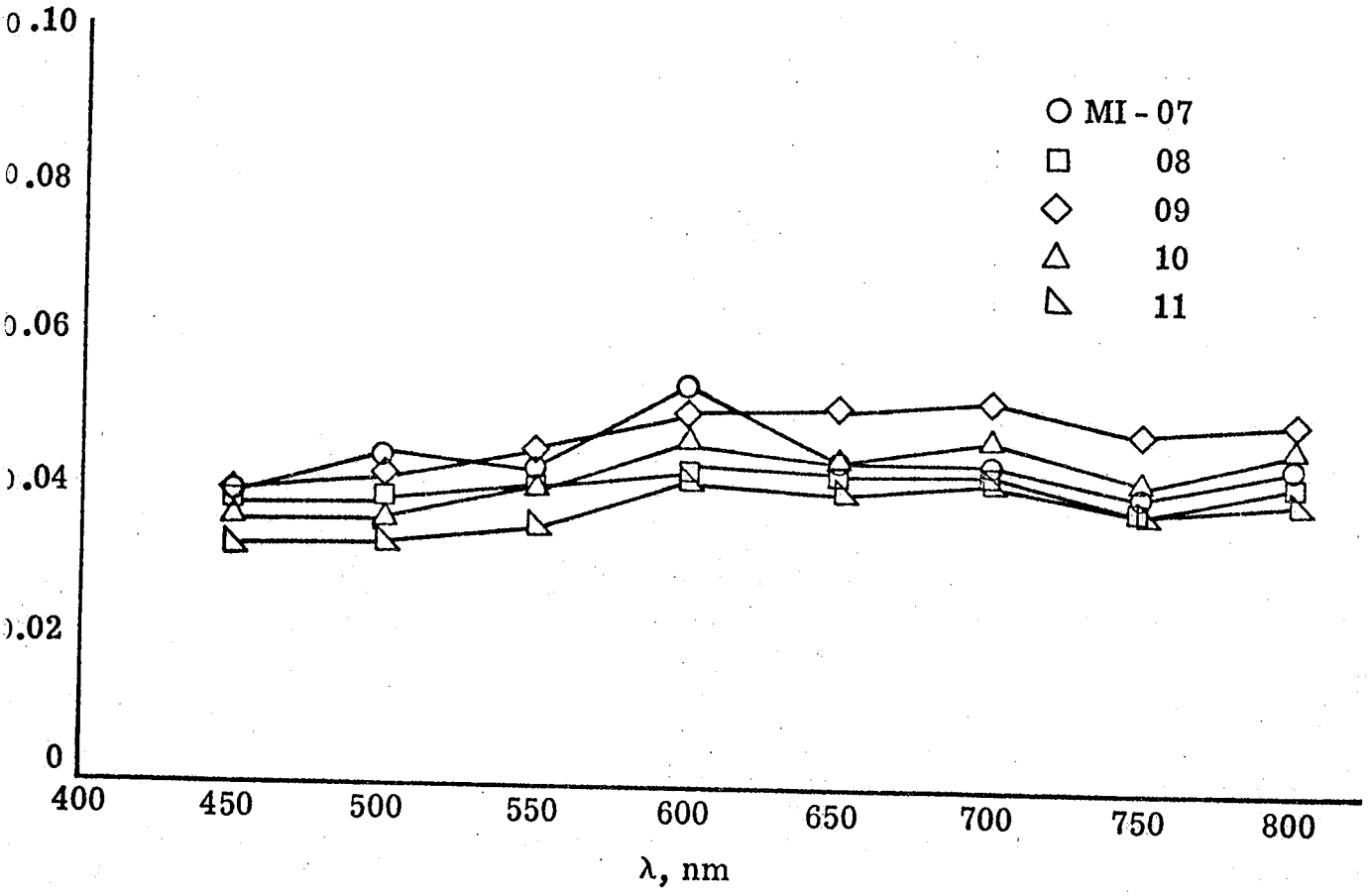

(b) b*/s

Figure 8.- Concluded.

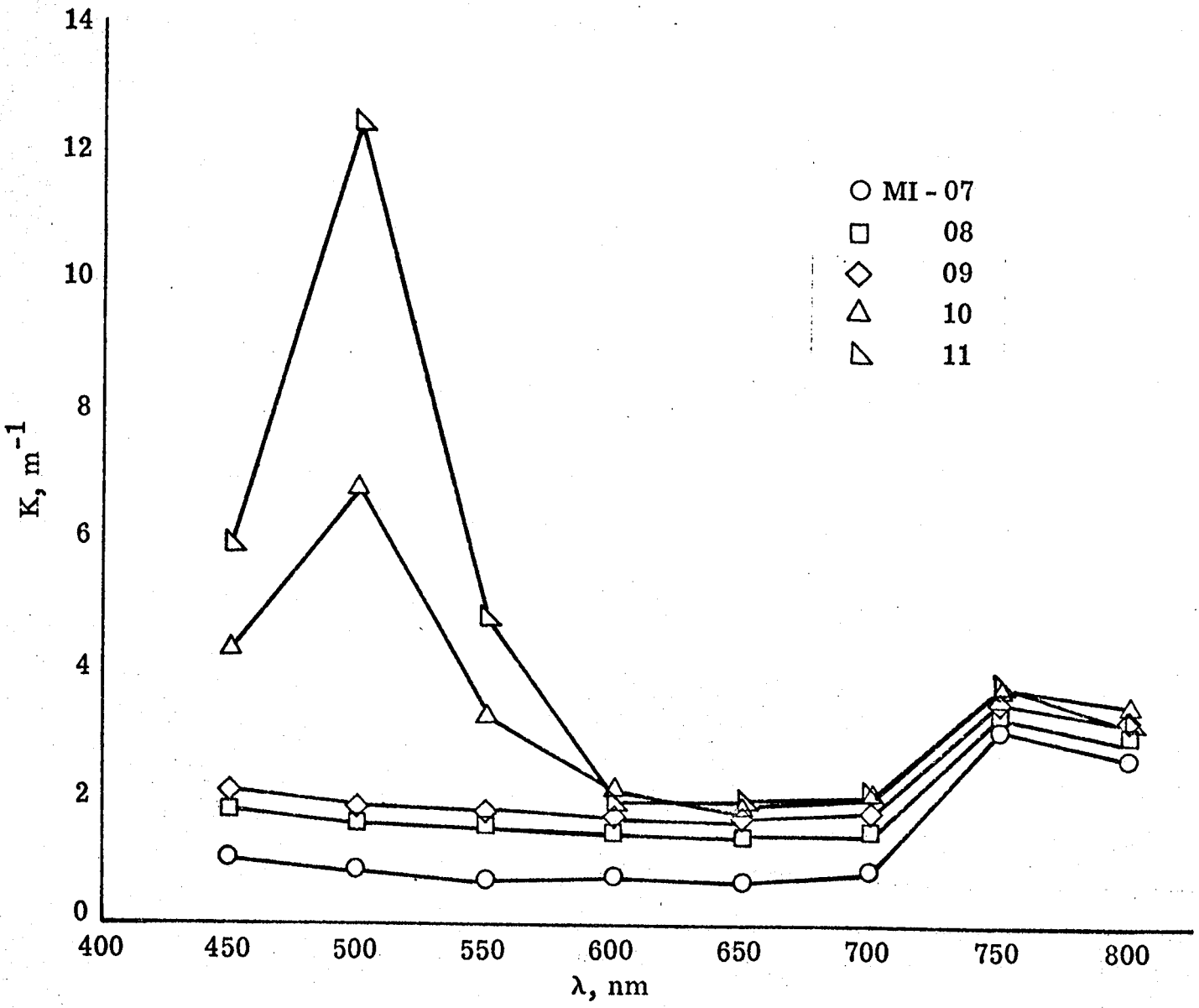

Figure 9.- Diffuse attenuation coefficient.

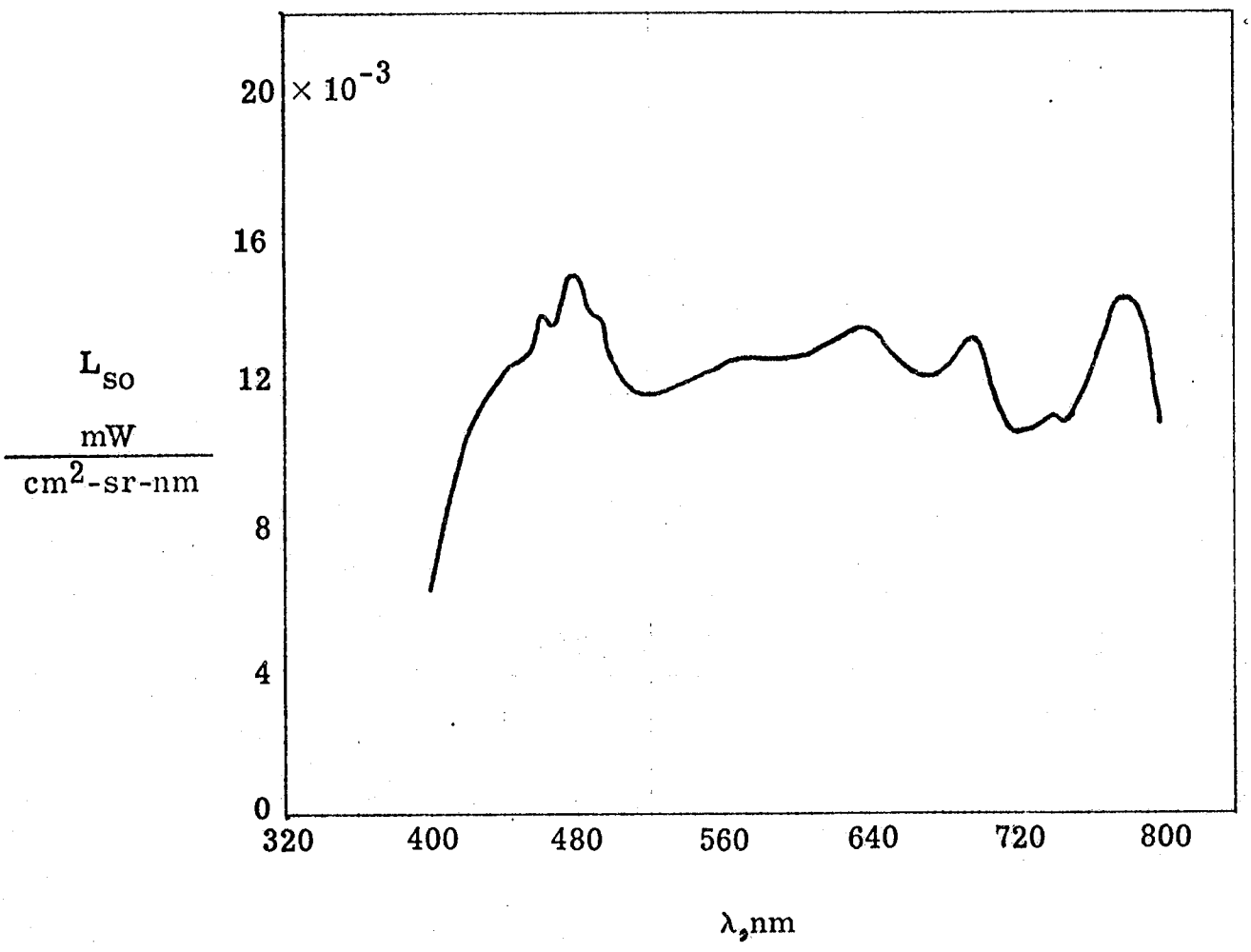

Figure 10.- White card radiance versus wavelength.

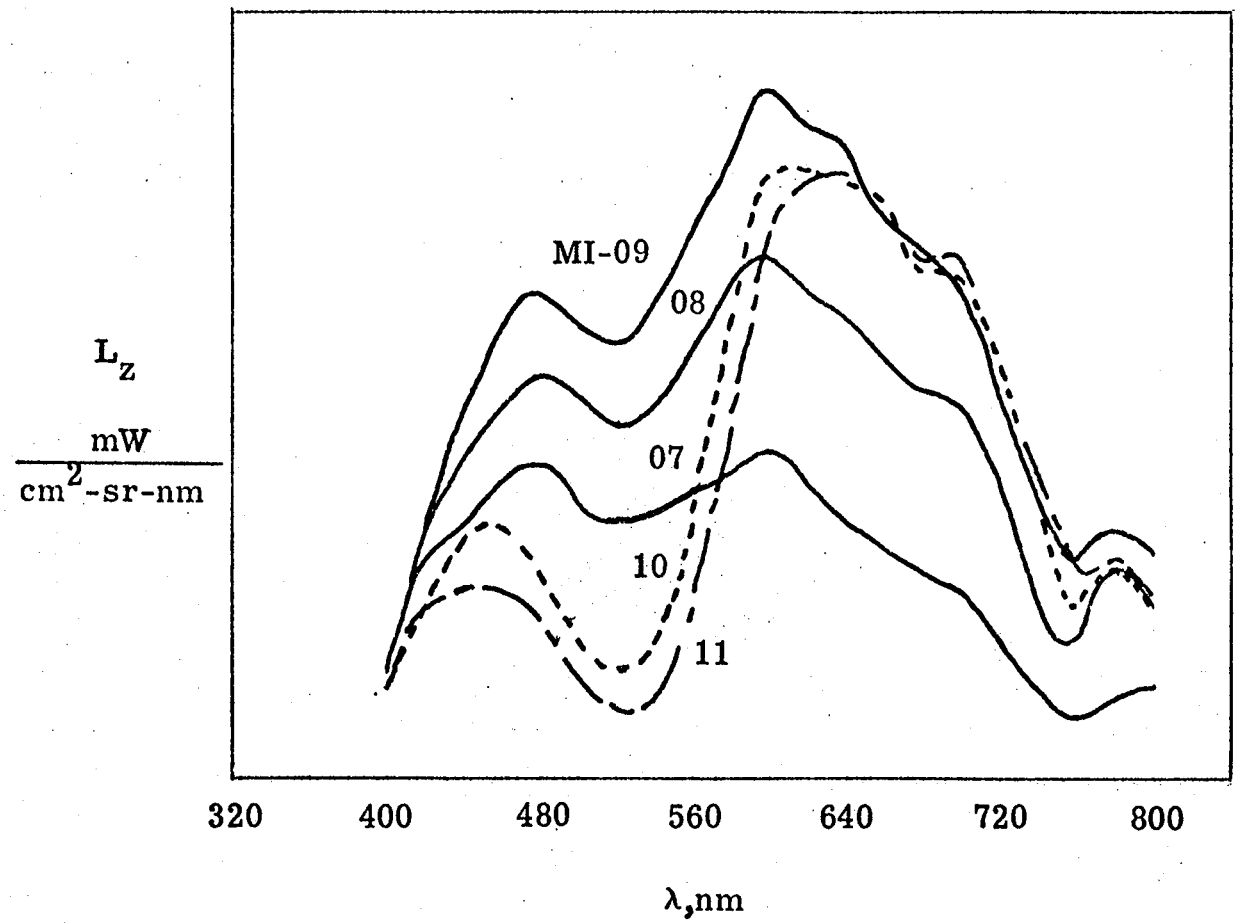

Figure 11.- Upwelled radiance versus wavelength for each mixture.

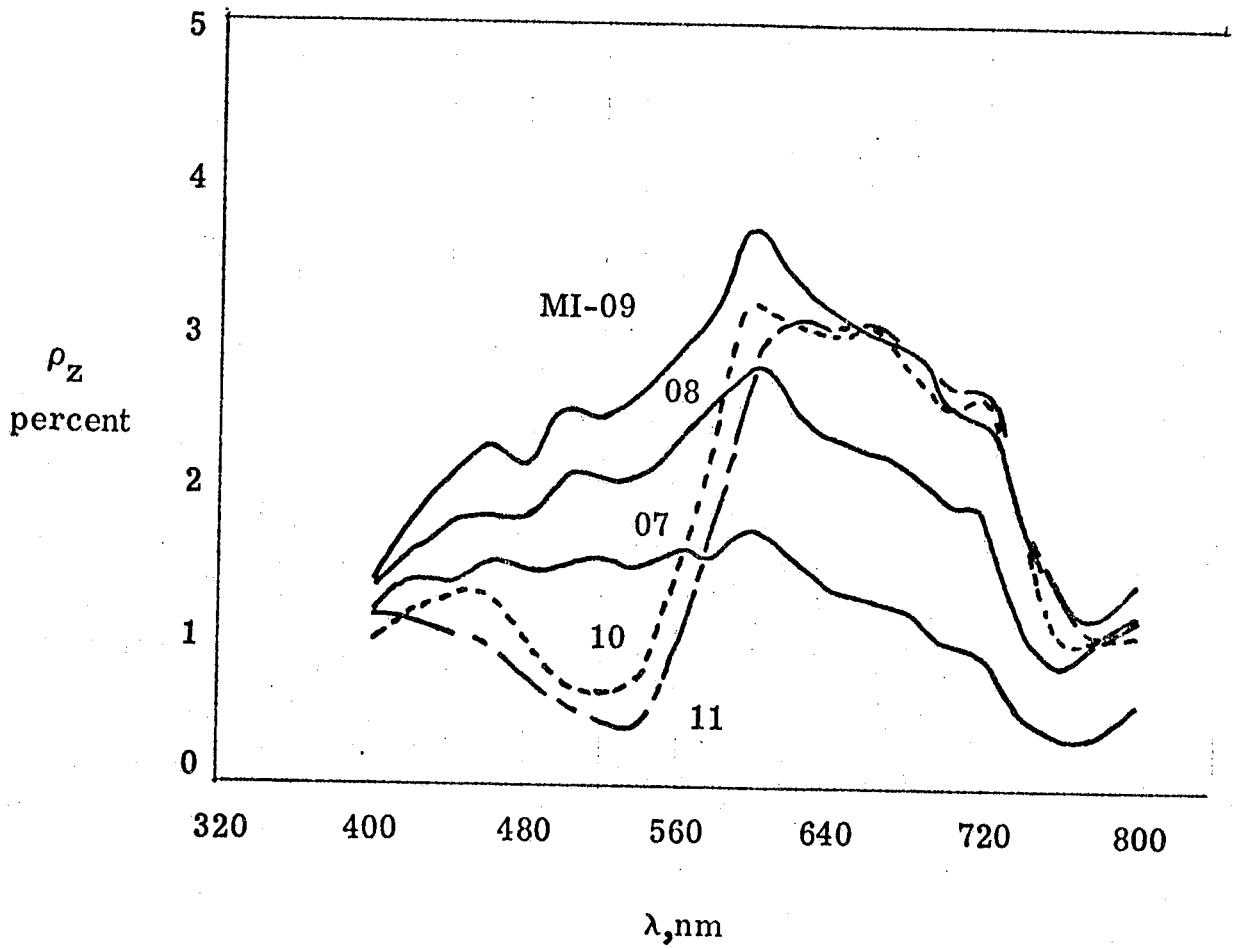

Figure 12.- Reflectance versus wavelength for each mixture.

1. Report No.	2. Government Accession No.	3. Recipient's Catalog No.
NASA TM-81896		

4. Title and Subtitle	5. Report Date
Laboratory Measurements of Selected Optical, Physical, Chemical, and Remote-Sensing Properties of Five Water Mixtures Containing Calvert Clay and a Nonfluorescing Dye	January 1981
	6. Performing Organization Code: 146-40-15-01

7. Author(s)	8. Performing Organization Report No.
J. W. Usry, C. H. Whitlock, L. R. Poole, and W. G. Witte, Jr.	
	10. Work Unit No.

9. Performing Organization Name and Address	11. Contract or Grant No.
NASA Langley Research Center Hampton, Virginia 23665	
	13. Type of Report and Period Covered: Technical Memorandum

12. Sponsoring Agency Name and Address	14. Sponsoring Agency Code
National Aeronautics and Space Administration Washington, DC 20546	

15. Supplementary Notes

16. Abstract

Remotely sensed spectral radiance, optical properties, and limited chemical and physical properties were measured in the laboratory for three mixtures containing filtered, deionized water and Calvert clay and two mixtures containing filtered, deionized water, Calvert clay, and a nonfluorescing dye. Total suspended solids concentrations ranged from 6.1 ppm to 24.3 ppm and sizes ranged between 1.5 μm and 10 μm with the most frequently occurring size less than 2 μm. Iron concentration was less than 1 percent of the total suspended solids. Nonfluorescing dye concentrations of the two mixtures were 20 ppm and 40 ppm. Attenuation coefficient for the five mixtures ranged from 4.8 m^{-1} to 21.3 m^{-1}. Variations in volume scattering function with phase angle were typical. Variations in attenuation and absorption coefficient with wavelength were similar for the mixtures without the dye. Attenuation coefficient of the mixtures with the dye increased for wavelengths less than 600 nm due to the dye's strong absorption peak near 500 nm. Reflectance increased as the concentration of Calvert clay increased and peaked near 600 nm. The nonfluorescent dye decreased the magnitude of the peak, but had practically no effect on the variation for wavelengths greater than 640 nm. At wavelengths less than 600 nm, the spectral variations of the mixtures with the dye were significantly different from those mixtures without the dye.

17. Key Words (Suggested by Author(s))	18. Distribution Statement
Remote Sensing Water Quality Optical Coefficients	Unclassified - Unlimited Subject Category 45

19. Security Classif. (of this report)	20. Security Classif. (of this page)	21. No. of Pages	22. Price*
Unclassified	Unclassified	40	A03

For sale by the National Technical Information Service, Springfield, Virginia 22161